Spring 5-4-2024

Healthy Aging Modulates the Neural Oscillatory Activity Underlying Basic Visual Processing and Verbal Working Memory

Seth D. Springer
University of Nebraska Medical Center

HEALTHY AGING MODULATES THE NEURAL OSCILLATORY ACTIVITY UNDERLYING BASIC VISUAL PROCESSING AND VERBAL WORKING MEMORY

By

Seth D. Springer

A DISSERTATION

Presented to the Faculty of the Graduate College at the University of Nebraska

In Partial Fulfillment of Requirements

For the Degree of Doctor of Philosophy

Interdisciplinary Graduate Program in Biomedical Sciences

(Neuroscience)

Under the Supervision of Drs. Tony Wilson and Pam May-Weeks

University of Nebraska Medical Center

Omaha, Nebraska

February, 2024

Supervisory Committee:

Elizabeth Heinrichs-Graham, Ph.D.

Daniel Murman, M.D.

Alfred Fisher, M.D., Ph.D.

ACKNOWLEDGEMENTS

There are many people who I need to thank for where I am today. Above all, I am thankful for my loving and supporting family. Principally, my wife and best friend Emily, who has been with me since the beginning of my undergraduate career. She has been my rock who has kept me grounded through these long years of study. Further, I am extremely thankful for our incredible son, Sylas, who is the light of my life and makes all of this work worth while. I am very thankful for my parents, Deni and Jeff Springer, who helped guide me to be the person I am today, as well as my loving siblings, Noah and Jersey. Finally, I am thankful for my undergraduate mentor, Dr. Allen Thomas, who instilled in me a love for academic research and drove me to pursue my PhD.

Much of my success during my graduate training can be attributed to being a part of such a productive and collaborative laboratory of scientists, led by my dedicated mentor, Dr. Tony Wilson. Despite his demanding schedule, Dr. Wilson always makes himself available for his students and he provided me with constant support and motivation. I extend my gratitude to my supervisory committee members Drs. Elizabeth Heinrichs-Graham, Pam May-Weeks, Daniel Murman, and Alfred Fisher; all of whom guided my graduate training, helping me on my journey towards becoming a physician-scientist.

I am also thankful for all of current and former colleagues and mentors at the Institute for Human Neuroscience including Mikki Schantell, Abraham Killanin, Jake Son, Maggie Rempe, Kellen McDonald, Yasra Arif, Morgan Busboom, Thomas Ward, Chloe Meehan, Augusto Diedrich, Cooper Livermore, Nathan Petro, Ilenia Salsano, Giorgia Picci, Brittany Taylor, Max Kurz, Gaelle

Doucet, Christine Embury, Alex Wiesman, Rachel Spooner, Nicholas Christopher-Hayes, Nichole Knott, Rebecca Losh, Melissa Welch, Lisa Houseman, Hannah Okelberry, and Grant Garrison for their academic support and friendship during my graduate training.

This research was financially supported by grants to my advisor, Dr. Tony Wilson, from the National Institutes of Health (R01-MH116782, R01-MH118013, P20-GM144641), including three administrative supplements to these awards. Additionally, my training was supported by a Ruth L. Kirschstein Predoctoral Fellowship from the National Institute on Aging (F30-AG076259) and supplemented by a research award from the Nancy and Ronald Reagan Alzheimer's Scholarship Fund. Finally, it is critical to thank the participants who make our research possible.

ABSTRACT

Worldwide economic and medical improvements have led to profound demographic shifts towards an older overall population. Unfortunately, with older age comes a variety of neurological changes which act to decrease individual quality of life and independence. Since the advent of functional neuroimaging, investigation of age-related changes in neural activity has been of particular interest. However, changes in population-level neural *dynamics* with age remain poorly characterized. Herein, we utilized magnetoencephalography (MEG), comprehensive neuropsychological assessments, and advanced analytical techniques to investigate spectrally-specific changes in neural oscillatory activity in a healthy aging population. First, we examined age-related deficiencies in visual processing using a well-established visual entrainment paradigm (Chapter 1). Next, we used a more complex visual grating paradigm to allow us to characterize age-related changes in visual gamma oscillations, as well as how these changes relate to individual processing speed (Chapter 2). Finally, we extended our investigation into higher-order cognition by utilizing a Sternberg working memory paradigm (Chapter 3). Overall, these results provide novel insights into the oscillatory underpinnings of age-related changes in cognition and serve as a foundation for future research into oscillatory deficits in patients affected by neuropsychological disorders which are prevalent in older individuals (e.g., Alzheimer's disease, Parkinson's disease, Dementia with Lewy Bodies).

TABLE OF CONTENTS

LIST OF FIGURES

LIST OF TABLES

LIST OF ABBREBIATIONS

AD	Alzheimer's disease
ADHD	Attention-deficit/hyperactivity disorder
CI	Confidence interval
CRUNCH	Compensation-related utilization of neural circuits hypothesis
CSF	Cerebrospinal fluid
CV	Coefficient of Variation
dlPFC	Dorsolateral prefrontal cortex
ECoG	Electrocorticography
EEG	Electroencephalography
ERP	Event-related potential
fMRI	Functional magnetic resonance imaging
HAROLD	Hemispheric asymmetry reduction in older adults
ITPL	Inter-trial phase locking
JASP	Jeffrey’s amazing statistical program
LCMV	Linearly constrained minimum variance
LFP	Local field potential
MEG	Magnetoencephalography
MFG	Middle frontal gyrus
PASA	Posterior-anterior shift in aging
PET	Positron emission tomography
PFC	Prefrontal cortex
SD	Standard deviation
SEM	Standard error of the mean
VWM	Verbal working memory

INTRODUCTION

Aging and Associated Changes to Cognition:

Over the past century, the global population has experienced a dramatic demographic shift towards an older life expectancy due, in large part, to advances in medicine and economic development (1). Unfortunately, even in the absence of pathologic processes, aging is associated with a variety of cognitive changes. Importantly, the rate of age-related cognitive decline is highly domain specific, with some steadily declining throughout all of adulthood while others showing little to no change until later adulthood (i.e., ~60-70 years; 2, 3, 4). When discussing cognitive domains which change with age, these domains are commonly grouped into fluid and crystallized abilities (5). Fluid abilities are those which require active processing of new information at the time of examination and include domains such as processing speed, working memory, and visuospatial processing. Crystallized abilities primarily depend on the use of previously acquired knowledge and represent one's ability to recall topics such as language (i.e., syntax and vocabulary) and general information (e.g., historical details and scientific facts). Previous research has demonstrated that healthy aging is associated with declines in fluid abilities throughout adulthood, whereas crystallized abilities have been shown to increase through later adulthood (i.e., ~70) before plateauing (2, 4, 6). The study of these age-related cognitive changes, and their neural correlates, is crucial as these cognitive functions are pivotal for maintaining a high quality of life and functional independence in aging individuals.

Age-Related Changes to Neural Structure and Function:

Structurally, healthy aging is associated with a variety of gross anatomical changes in both the gray and white matter. Across the entire brain, older adults tend to have less gray matter, volume and thickness, than those of younger adults (7). Interestingly, this loss of gray matter is largely not due to neuronal cell loss. Instead, this

gray matter atrophy is associated with degeneration of dendritic arborization (e.g., decreased number of dendritic spines and dendritic shortening; 8, 9), ultimately leading to reductions in total synaptic density. Beyond gray matter alterations, healthy aging is also associated with white matter changes including decreases in white matter volume and increases in the number of white matter lesions (7). These white matter changes are related to the dysfunction of both neurons (e.g., axonal and myelination loss) and glial cells (e.g., astrocytic gliosis), and are predictive of poor performance on tasks of processing speed, executive function, and memory (10). Interestingly, the spatial specificity of age-related gray and white matter abnormalities are quite similar, with prefrontal cortical regions affected the most, followed by temporal and parietal cortices, and leaving the occipital cortices relatively spared (7, 11, 12).

Considering the well-documented age-related declines in fluid cognitive abilities and structural neural degeneration, early researchers investigating functional neural activity in older participants expected to find patterns of decreased activation as a function of age (13). Instead, initial positron emission tomography (PET) and functional magnetic resonance imaging (fMRI) studies revealed robust age-related increases in activity, particularly in prefrontal cortical areas and sometimes involving bilateral hemispheric recruitment (14-16). Since then, these results have been replicated and expanded upon; notably, two large scale fMRI meta-analyses demonstrated age-related increases in activity in fronto-parietal areas and decreases in occipital regions during a variety of different cognitive tasks (17, 18). Several highly influential theories have been proposed to explain these age-related changes in neural activity, including the Hemispheric Asymmetry Reduction in Older Adults (HAROLD) theory, the

Posterior-Anterior Shift in Aging (PASA) model, and the Compensation-Related Utilization of Neural Circuits Hypothesis (CRUNCH).

The first of such theories was the HAROLD model which proposed that, under similar cognitive loads, older individuals would display less lateralized (i.e., more bilateral) prefrontal cortical (PFC) activity compared to younger individuals (14). Further, it was suggested that these age-related decreases in PFC lateralization might reflect either neural compensation (i.e., greater recruitment of neural resources to maintain adequate functionality) or dedifferentiation of cognitive abilities (i.e., the loss of functional specialization of cortical regions; 14). Next came the PASA model, which focused on the observation that age-related increases in frontal cortical activity are often accompanied by decreases in posterior cortical (i.e., occipito-temporal) activity, and that the frontal overactivation may be compensatory to offset the posterior sensory deficits (19). Finally, CRUNCH proposed that, at any age, individuals would recruit additional neural circuitry to meet increasingly difficult task demands (20). Critically, CRUNCH posited that older individuals would display greater neural activity, relative to younger individuals, at all task difficulties. However, as task difficulty increases, an inflection point (i.e., "CRUNCH point") would be reached in which older participants exhaust their ability to recruit additional neural resources for compensation, resulting in declining task performance and decreased levels of neural activity. Each of these theories is supported by a plethora of previous research across a variety of different neuroimaging modalities (e.g., PET, fMRI, EEG, MEG) and in many cognitive domains (e.g., working memory, attention, visuospatial processing) (13, 14, 19-23).

Neural Oscillations:

Neural oscillations are the rhythmic fluctuations in dendritic membrane potentials which are the result of intrinsic cellular properties and population-level neural activity (24), and can be measured using local field potentials (LFP), electrocorticography

(ECoG), electroencephalography (EEG), and magnetoencephalography (MEG). These oscillations are typically grouped into several canonical bands, including delta (~1-3 Hz), theta (~4-7 Hz), alpha (~8-12 Hz), beta (~15-30 Hz), and gamma (>30 Hz). Each of these frequency bands have unique cortical distributions and are associated with distinct cognitive functions (25). Alterations to cortical oscillatory activity have been linked to a variety of neuropsychiatric disorders, including schizophrenia (26), autism (27), Parkinson's disease (28), and Alzheimer's disease (29). Despite the clear clinical utility of neural oscillations, to date, research investigating oscillatory changes as a function of healthy aging is relatively sparse.

Resting-state electrophysiological analyses have demonstrated age-related decreases in lower frequency activity (i.e., delta and theta) and increases in higher frequency activity (i.e., beta and gamma; 25, 30). Further, healthy aging has been associated with decreases in peak alpha frequency (31), however, results from analyses of age-related changes in alpha activity remain quite mixed (25, 30, 32). Results from task-based oscillatory analyses of healthy aging have largely supported the major neurocognitive theories of aging (i.e., HAROLD, PASA, and CRUNCH). Specifically, across several frequency bands (i.e., theta, alpha, beta, and gamma), these electrophysiological analyses have demonstrated age-related increases in higher-order cognitive regions (particularly in prefrontal areas) (33-38), increases in bilateral prefrontal cortical recruitment (35), and a shifting of activity away from posterior regions towards more anterior regions (e.g., weaker posterior activity and stronger frontal activity) (39-45). Despite the utility of the existing healthy aging electrophysiologic literature, the vast majority of this previous work was done using sensor-level

data. As such, the cortical generators of these age-related oscillatory changes remain largely poorly characterized.

Neuroimaging using Magnetoencephalography:

Magnetoencephalography is a passive and noninvasive neuroimaging technique which utilizes an array of superconducting sensors to measure the minuscule magnetic fields (i.e., ~10^{-15} T) that are produced by population-level neural activity. As such, similar to EEG and in contrast to fMRI, MEG directly measures neural activity with excellent temporal resolution (i.e., millisecond). Importantly, unlike electric fields, magnetic fields are not distorted by the intervening tissues (e.g., scalp, skull, CSF), which have a wide range of different conductivity values. Thus, MEG provides better spatial precision for source reconstruction compared to EEG. The combination of good spatial precision and excellent temporal resolution afforded to MEG makes it an ideal neuroimaging modality for the characterization of neural oscillatory activity.

Goals of the Current Study:

The current studies aim to fill knowledge gaps regarding frequency-specific changes in neural oscillatory activity across the adult lifespan using advanced neuroimaging techniques. Specifically, we aim to characterize age-related changes in the oscillatory mechanisms underlying basic visual processing using a visual entrainment paradigm (Chapter 1) as well as a more complex grating stimulus (Chapter 2). Additionally, we aim to investigate the effects of healthy aging on the oscillations during each phase of working memory processing (i.e., encoding, maintenance, and retrieval). From these results, we expect to develop a better understanding of how healthy aging affects neurophysiological processes ranging in complexity from lower-order (Chapters 1 and 2) to higher-order (Chapter 3) operations. Furthermore, these studies will provide much needed background to guide future research into the

oscillatory aberrations associated with neurodegenerative processes, which become more prevalent with increasing age (e.g., Alzheimer's disease, Parkinson's disease).

CHAPTER 1: VISUAL ENTRAINMENT DEFICITS IN HEALTHY AGING ADULTS

The material presented in this chapter was previously published in Springer, Erker, Schantell, Johnson, Willett, Okelberry, Rempe, and Wilson, 2023, Disturbances in Primary Visual Processing as a Function of Healthy Aging, Neuroimage, 271:120020

Introduction:

Aging, even in the absence of pathological changes, has been shown to affect a variety of visual processes, including visual acuity (46), motion perception (47), and contrast sensitivity (48, 49). These changes in visual processing during healthy aging are the result of complex and multifaceted alterations along the entire visual pathway; from the cornea to the visual cortices (50). Understanding the nature of visual processing deficits in aging is critical considering that decrements in basic visual processing have been shown to significantly decrease the quality of life of older adults (51) and can lead to increased risk of injury (e.g., via falling or accidents while driving; 52, 53, 54).

A common neurological change associated with healthy aging is the gradual decrease of cortical thickness across the whole brain (55, 56). Though general age-related decreases in cortical thickness have been commonly reported, analyses tend to show less occipital cortical thinning relative to other cortical areas (11, 57-60). Importantly, variation in cortical thickness, as a function of aging, pathological processes, or individual differences, have been shown to correlate with altered neural activity in the same regions (61-65). Though previous research has demonstrated the interrelated nature of healthy aging, decreased cortical thickness, and alterations in neural activity, the relationship between these variables has yet to be thoroughly investigated, and this is especially true for the visual cortex.

To date, the majority of aging studies investigating visual cortical responses have demonstrated significant changes in the characteristics of these responses. Most notably, studies using electroencephalography (EEG) and magnetoencephalography

(MEG) have shown that electrode/sensor level responses to visual stimulation in older adults tend to have lower amplitudes (66-69) and greater latencies compared to those observed in younger individuals (66, 68, 70-74). While these findings of decreased visual response amplitudes and increased latencies are robust in the electrophysiological literature (e.g., EEG and MEG), studies using functional MRI (fMRI) have been less consistent with some studies supporting the EEG/MEG findings (75-78) and many others finding no changes in visual response characteristics as a function of healthy aging (79-81). These discrepancies could be partially attributable to differences in spatial scales, as the EEG and MEG studies that have consistently found age-related effects in visual responses are generally those that relied on sensor/electrode level analyses, which typically reflect responses over more widespread brain regions than is the case with fMRI and source-resolved MEG/EEG. Thus, the anatomical origins of these aging effects and their relationship to observations from fMRI remain poorly understood.

While visual entrainment paradigms have been used in clinical neuroscience research for over 20 years, interest has sharply increased recently due to new evidence suggesting that such entrainment may attenuate beta amyloid plaques in mouse models of Alzheimer's disease (AD) and thus may hold significant therapeutic promise via the capacity to reduce a key pathological feature of the disease (82-84). Visual entrainment responses are generated when neurons in the visual cortices synchronize their firing with the frequency of a flickering visual stimulus. This visual response is unique, relative to non-flickering stimuli, as the neuronal activity is both time- and phase-locked to the visual stimulation and often exhibits an extended duration that matches that of the visual stimulation (85, 86). The use of sustained entrainment paradigms is

ideal for investigating visual processing because the elicited neural responses have high signal-to-noise ratios and the sustained nature of the response allows for time varying analysis of visual activity. Nonetheless, despite these advantages, most studies of visual processing in aging have used more simple tasks that involve transient flashes or similar stimuli and focused on the resulting evoke fields (MEG) or potentials (EEG). As briefly mentioned above, beyond aging and recent work in AD, visual (and auditory) entrainment paradigms have been widely used in clinical neuroscience and proven to be useful in the characterization of psychiatric and other neurological disorders (e.g., schizophrenia, autism, ADHD, and migraines; 87, 88-93). Further, some of these studies suggest that specific conditions like schizophrenia are associated with deficits in both visual (89, 90) and auditory domains (91, 94). However, beyond schizophrenia, the pattern is more unclear because less work has been performed. Interestingly, a recent study also showed that entrainment in one modality (e.g., visual) affects higher order processing of stimuli presented in other modalities (e.g., auditory; 95).

In sum, electrode/sensor-level electrophysiological responses serving visual processing using transient, non-flickering visual stimuli have been extensively studied in aging populations, but far less is known about how healthy aging affects cortical-level visual entrainment responses. Further, though cortical thickness changes have been shown to be strongly related to aging, data on the occipital cortex has been less robust and very few studies to date have attempted to link healthy aging to both cortical thinning and visual processing. Thus, in the current study, we examined the neural dynamics of visual entrainment responses using MEG in an aging sample, with an emphasis on neural response amplitude, latency, and consistency (i.e., inter-trial phase-locking and single-trial amplitude consistency). A key goal was to determine whether age-related differences in these response parameters are affected by other functional parameters (e.g., are differences in amplitude attributable to less consistent responses

from trial-to-trial) and/or cortical thickness. In order to produce the strongest neural responses, the frequency of entrainment was chosen to fall within the range that has been shown to elicit the most robust visual entrainment responses in healthy adults (i.e., 15 Hz; 96). Based on the broader visual processing literature, we hypothesized that, as a function of healthy aging, visual cortical responses would be less consistent, have decreased amplitudes, and increased latencies.

Methods:

Participants

A total of eighty adults with a mean age of 46.35 (SD = 13.50) years and a range of 20.22 to 67.00 years were selected for inclusion in this study. These participants were chosen from a larger-scale study of accelerated aging in persons with HIV, with only the HIV-negative participants included in this investigation of healthy aging. Among the included control participants, the number of participants per decade of life was relatively equal (i.e., uniform) and their level of education did not vary as a function of age ($F_{1,77}$ = 1.91; p = .171). Of the 80 adults, 76 (95%) were right-handed, 63 (79%) were male, 9 (11%) were Black, 5 (6%) were Asian, 63 (79%) were Caucasian, and the remaining 3 (4%) were more than one race, which corresponds closely to the racial demographics of the surrounding region. All included participants scored in the normal range on a neuropsychological testing battery that probed seven cognitive domains (i.e., processing speed, memory, learning, language, executive function, attention, and motor function). Exclusionary criteria included any medical illness affecting CNS function (e.g., HIV/AIDS, Lupus, etc.), any neurological or psychiatric disorder, cognitive impairment, history of head trauma, current substance abuse, and the MEG laboratory's standard exclusionary criteria (e.g., ferromagnetic implants). The Institutional Review Board reviewed and

approved this investigation. Each participant provided written informed consent following a detailed description of the study.

Experimental Paradigm

During the MEG recording, participants sat in a nonmagnetic chair within a magnetically shielded room and were instructed to fixate on an entrainment stimulus that flickered at a rate of 15 times per second (Hz). The stimulus was a small white circle, 3.8 cm in diameter that was presented centrally on a black background and subtended a visual angle of 1.83°. The duration of each flicker-train was 2500 ms and the inter-stimulus interval was randomly jittered between 2000 and 2500 ms. Each participant completed 120 trials, which resulted in a total recording time of about 9.5 minutes.

MEG Data Acquisition

MEG recordings were conducted in a one-layer magnetically shielded room with active shielding engaged to compensate for environmental noise. Neuromagnetic responses were continuously sampled at a rate of 1 kHz with an acquisition bandwidth of 0.1-330 Hz using an Elekta MEG system with 306 magnetic sensors (Helsinki, Finland). During data acquisition, participants were continually monitored via real-time audio-video feeds from inside the magnetically shielded room. MEG data were individually corrected for head motion and subjected to noise reduction using the signal space separation method with a temporal extension (97).

Structural MRI Acquisition, Processing, and MEG Coregistration

Preceding MEG recording, four coils were attached to the subject's head and localized, together with the three fiducial points and scalp surface, with a 3-D digitizer (FASTRAK 3SF0002, Polhemus Navigator Sciences, Colchester, VT, USA). Once the participants were positioned for MEG recording, an electric current with a unique frequency label (e.g., 321 Hz) was fed to each of the coils. This induced a measurable

magnetic field and allowed each coil to be localized in reference to the sensors throughout the recording session. Since coil locations were also known in head coordinates, all MEG measurements could be transformed into a common coordinate system. With this coordinate system, each participant's MEG data were co-registered with their structural T1-weighted MRI prior to source space analysis using BESA MRI (Version 2.0). All MRI data were aligned parallel to the anterior and posterior commissures and transformed into standardized Talairach space. Following source analysis (i.e., beamforming), each subject's 4.0 mm^3 functional MEG images were also transformed into standardized space using the transform that was previously applied to the structural MRI volume and spatially resampled to enable group-wise statistical comparisons.

MEG Preprocessing, Time-Frequency Transformation, and Sensor-Level Statistics

Cardiac and ocular artifacts (e.g., blinks and eye movements) were removed from the data using an adaptive spatial filtering approach which separates artifact and brain signal topographies, allowing for the removal of artifacts without distortion of the underlying neurological signals (98). This artifact correction was accounted for during source reconstruction. The continuous magnetic time series was then divided into epochs of 4400 ms duration, with the baseline extending from -600 to 0 ms prior to the onset of the flickering stimulus. Epochs containing remaining artifacts (after cardiac and ocular artifact removal) were rejected, per participant, using a fixed threshold method, supplemented with visual inspection. Across the sample, an average amplitude threshold of 1149.69 (SD = 367.05) fT and an average gradient threshold of 169.69 (94.75) fT/s was used to reject artifacts. An average of 108.15 (SD = 7.66) trials per participant were used for further analysis. Importantly, the amplitude and gradient thresholds used for artifact rejection and the total accepted trial count per participant did not differ as a function of age (*p*s > .280).

Artifact-free epochs (-600 to 3800 ms, with zero defined as flicker onset) were then transformed into the time-frequency domain using complex demodulation (99), with a time-frequency resolution of 0.5Hz/100ms and a bandwidth of 4-50 Hz. The resulting spectral power estimates per sensor were averaged over trials to generate time-frequency plots of mean spectral density per participant. These sensor-level data were then normalized using each respective frequency bin's baseline power, which was derived by averaging over the baseline time window (-600 to 0 ms).

The specific time-frequency windows used for subsequent sourcing imaging were determined by statistical analysis of the sensor-level spectrograms across all trials, gradiometers, and participants. Each data point in the spectrograms were initially evaluated using a mass univariate approach based on the general linear model. To reduce the risk of false-positive results while maintaining reasonable sensitivity, a two-stage procedure was followed to control type 1 error. In the first stage, paired-sample *t*-tests against baseline were conducted on each data point and the output spectrograms of *t*-values were thresholded at $p < .05$ to define time-frequency bins containing potentially significant oscillatory deviations across all participants. In stage two, the time-frequency bins that survived the threshold were clustered with temporally and/or spectrally neighboring bins that were also below the threshold ($p < .05$), and a cluster value was derived by summing all of the *t*-values of all data points in the cluster. Nonparametric permutation testing was then used to derive a distribution of cluster values, and the significance level of the observed clusters (from stage one) were tested directly using this distribution (100, 101). For each comparison, 10,000 permutations were computed to build a distribution of cluster values. Based on these analyses, the time-frequency windows that contained significant oscillatory events across all participants were subjected to a beamforming analysis. Thus, a data-driven approach was utilized for selecting time-frequency windows to be imaged.

MEG Source Imaging and Statistics

Cortical networks were imaged through an extension of the linearly constrained minimum variance vector beamformer known as dynamic imaging of coherent sources (102-104), which applies spatial filters to time-frequency sensor data in order to calculate voxel-wise source power for the entire brain volume. Such images are typically referred to as pseudo-t maps, with units (pseudo-*t*) that reflect noise-normalized power differences (i.e., active vs. baseline) per voxel. Following convention, the source power in these images was normalized per participant using a separately averaged pre-stimulus noise period (i.e., baseline) of equal duration and bandwidth (105). MEG preprocessing and source imaging used the Brain Electrical Source Analysis (version 7.0) software.

To assess the anatomical basis of the responses identified through the sensor-level analysis, the 3D beamformer output maps were averaged across all participants. To investigate the neural differences in visual processing as a function of healthy aging, virtual sensors (i.e., voxel time series data) were extracted from each participant's MEG data. Specifically, we identified the voxel with the strongest entrainment response in the grand-averaged image (i.e., across all participants and time windows) and computed virtual sensors for that location by applying the sensor weighting matrix derived from the forward solution to the preprocessed signal vector, which yielded a time series for the specific voxel in source space. For this coordinate of interest, the envelope of spectral power was computed for the frequency range used in the beamforming analysis (i.e., 14.5-15.5 Hz, see below). For each participant, the mean baseline activity was derived by averaging the absolute amplitude time series data across the baseline period (-600 to 0 ms). To derive the relative response time series, the absolute amplitude time series was normalized using the same -600 to 0 ms baseline period. Estimates of the relative entrainment response were derived by averaging the relative amplitude time series of

the peak voxel across the significant time window derived from the sensor-level data (i.e., 200 to 2600 ms). Further, visual entrainment response latency was determined for each participant by calculating the time it took for them to reach 50% of their maximum entrainment response. Additionally, using these same peak voxel time series, the inter-trial phase locking (ITPL) value was computed per participant for the time-frequency range used in the beamforming analysis (i.e., 14.5-15.5 Hz; 200 to 2600 ms) to assess phase consistency. Finally, to evaluate the consistency of visual entrainment amplitudes across trials, the coefficient of variation was calculated across the single-trial responses for each participant. To reduce the impact of outliers on statistical analyses, participants with values 2.5 SDs above or below the group mean were excluded for each analysis.

Cortical Thickness Processing

To examine cortical thickness, the T1-weighted MRI data were then processed using additional surface-based morphometry calculations in the computational anatomy toolbox (CAT12 v12.6; 106) at a resolution of 1 mm^3. This method uses a projection-based thickness approach to estimate cortical thickness and reconstruct the central surface in one step (107). Briefly, following tissue segmentation, the white matter distance is estimated, and the local maxima are projected onto other gray matter voxels using a neighboring relationship described by the WM distance. This method accounts for partial volume correction, sulcal blurring, and sulcal asymmetries. Topological defects are corrected based on spherical harmonics (108) and the cortical surface mesh was reparametrized into a common coordinate system via an algorithm that reduces area distortion (109). Finally, the resulting maps were resampled and smoothed using a 15 mm FWHM Gaussian kernel. These cortical thickness maps were then parcellated using the Desikan-Killiany (DK) atlas. Subject-wise cortical thickness values were extracted in several ways: 1) averaged across all atlas regions (i.e., entire cortex), 2) averaged

across occipital atlas regions (i.e., lingual, pericalcarine, lateral occipital, and cuneus), and 3) primary visual cortex only (i.e., V1; bilateral pericalcarine regions). The three participants without high quality structural MRI data were excluded from these analyses.

Statistical Analyses

All statistical analyses were performed using *R* (110), and data plots were generated using *ggplot2* (111). In order to perform the mediation analysis, the PROCESS macro (112) for *R* was utilized, with indirect effects estimated using bootstrapping (113). Linear regression analyses were used to test for differences as a function of healthy aging in mean baseline amplitude, relative entrainment amplitude, response latency, average inter-trial phase locking, average entrainment amplitude variability (coefficient of variation), and cortical thickness (i.e., across the entire cortex, occipital cortex, and pericalcarine region). To ensure that age-related changes in occipital cortex and pericalcarine cortical thickness were not responsible for age-related changes in visual entrainment response metrics, linear regression analyses were used to model the relationship between cortical thickness and the visual response metrics. Additionally, inclusion of these cortical thickness measures as nuisance covariates in all reported statistical models did not change the significance or interpretations of any results. Finally, permutation testing of the relative entrainment time series was performed using custom MATLAB scripts (114).

Results:

Cortical thickness analysis

As detailed in the methods section, cortical thickness estimates were parcellated using the DK atlas. Subject-wise cortical thickness values were then averaged across the entire cortex, the bilateral occipital cortices (i.e., lingual, pericalcarine, lateral

occipital, and cuneus), and the bilateral pericalcarine regions. We found significant age-related decreases in cortical thickness across the entire cortex ($F_{1,74}$ = 10.53, p = .002), bilateral occipital cortex ($F_{1,74}$ = 5.81, p = .018), and pericalcarine regions ($F_{1,74}$ = 8.74, p = .004).

Sensor-level analysis

Sensor-level time-frequency analysis across all participants revealed significant oscillatory responses in a large number of posterior sensors at the base entrainment frequency (i.e., 15 Hz) and harmonics (i.e., 30 and 45 Hz), all of which were increases in amplitude relative to baseline (Figure 1A). Given the goals of the study, we focused on the base-frequency entrainment response at 15 Hz, which began at about 200 ms after the presentation of the flickering stimulus and remained significantly different from

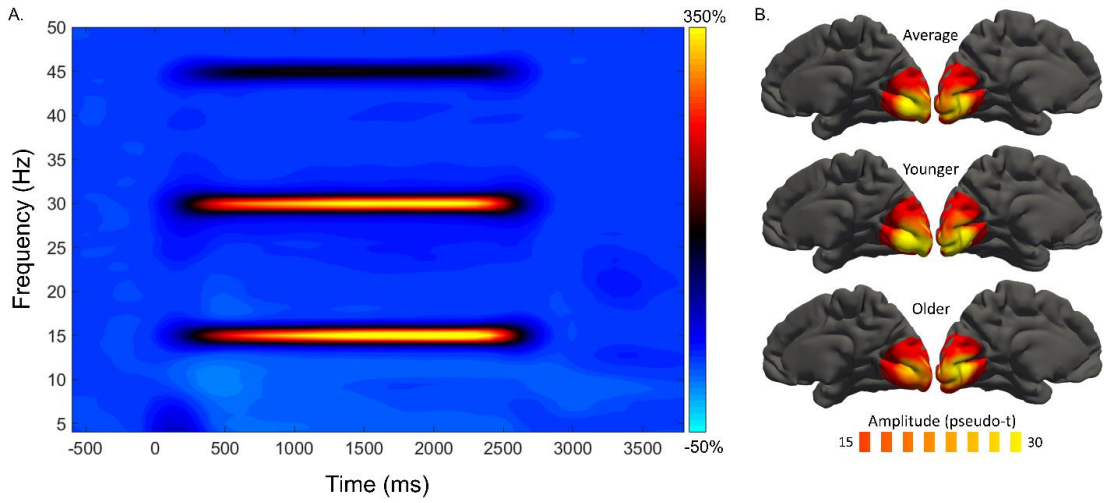

Figure 1. Sensor- and source-level activity during visual entrainment.

A. Grand-averaged time-frequency spectrogram from a sensor near the occipital cortex (i.e., MEG2123), with time (ms) shown on the x-axis and frequency (Hz) denoted on the y-axis. A color scale bar shown to the right of the spectrogram denotes the percent power change relative to the baseline period (-600 to 0 ms). There is clear entrainment to the 15 Hz flicker stimulus and harmonics (i.e., 30 and 45 Hz). B. Mean beamformer images (pseudo-*t*; see color bar) of the 15 Hz entrainment response (i.e., 200-2600 ms and 14.5-15.5 Hz). The images labeled "younger" and "older" represent the average source representations for the youngest and oldest participants, as determined with cutoffs of less than or greater than 0.5 standard deviations from the mean age, respectively. Note that all statistical analyses treated age as a continuous variable and the subgroups here are just for illustration purposes.

baseline until tapering off around 100 ms following its removal (i.e., 200-2600 ms; $p <$ .001, corrected).

Beamformer and Virtual Sensor Analysis

To determine the cortical origins of the base-frequency entrainment response, we imaged the significant sensor-level time-frequency bin (i.e., 200-2600 ms and 14.5-15.5 Hz) in each participant using a frequency-resolved beamformer. Since our baseline was only 600 ms in duration, we used four non-overlapping time windows to image the full 200-2600 ms response and then averaged these four images in each participant. In agreement with previous studies of visual entrainment, strong increases in narrow-band 15 Hz activity were observed in the bilateral primary visual cortices (Figure 1B). As stated in the methods, we extracted time series data from the peak voxel in the grand-averaged image and then computed the mean relative response amplitude to the flicker stimulus (i.e., 200 to 2600) and the mean absolute amplitude during the baseline period (-600 to 0 ms) to estimate the strength of spontaneous activity. Across the sample, mean entrainment responses became significantly weaker as a function of age ($F_{1,77} = 4.46$, $p = .038$; Figures 2 and 3A). In contrast, the strength of spontaneous activity during the baseline did not differ as a function of age ($F_{1,77} = 0.04$, $p = .838$; Figure 3B). Further, mean entrainment responses were not found to be related to visual cortical thickness (occipital cortex: $F_{1,72} = 2.27$, $p = .137$; pericalcarine region: $F_{1,72} = 1.76$, $p = .189$). Note that for these analyses we focused on the two occipital regions since these areas pertain to the origins of the neural responses.

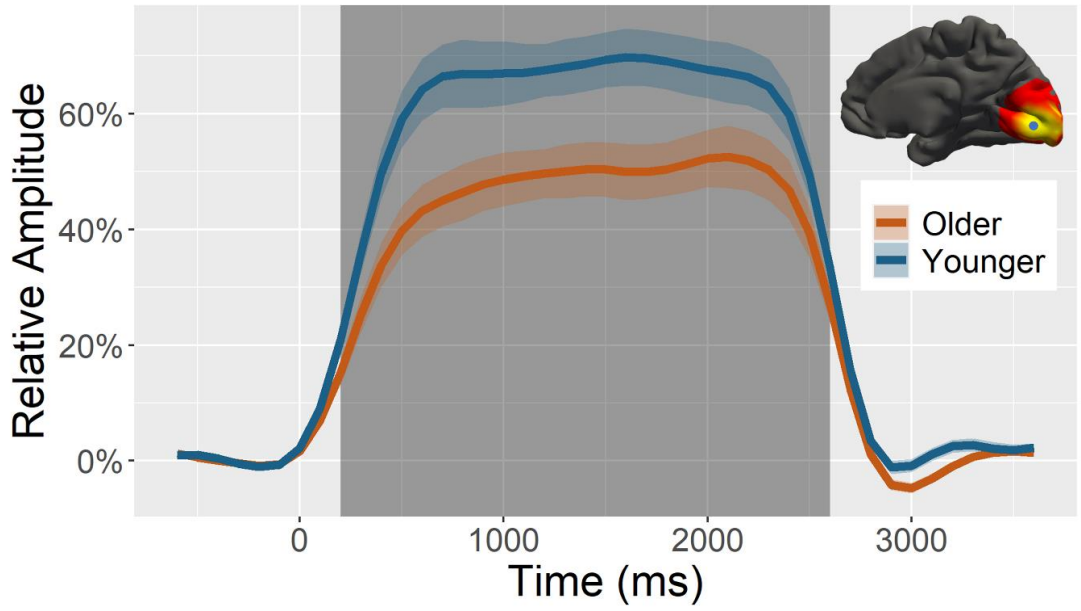

Figure 2. Relative amplitude of 15 Hz primary visual responses.

From the peak voxel exhibiting the strongest neural activity in response to the 15 Hz entrainment stimulus (blue dot within inset image), relative time series (i.e., baseline-corrected) were extracted to evaluate differences in entrainment response amplitude as a function of age during the time window identified through the sensor-level analysis (i.e., 200-2600 ms; shaded area). Note that all statistics treated age as a continuous variable, but for the sake of visualization participants have been dichotomized in this figure using a 0.5 SD from the mean cutoff.

Next, to investigate the temporal dynamics of the entrainment response, we regressed the latency of the response onto participant age (Figure 3C). We defined the response latency by finding the peak amplitude in each participant and then computing the time it took to reach 50% of that peak in each participant. We found that as age increased, participants took significantly longer on average to entrain to the flickering stimulus ($F_{1,69}$ = 6.06, p = .016). We then tested for aging effects on the consistency of the entrainment response amplitude using the coefficient of variation (CV) and phase using the ITPL value (Figures 3D and 3E, respectively). There were no aging effects in the consistency of the cross-trial amplitude ($F_{1,76}$ = 3.22, p = .077) nor phase ($F_{1,78}$ = 1.05, p = .309). Further, there was no significant relationship between visual cortical thickness and latency (occipital cortex: F_{66} = 2.75, p = .102; pericalcarine region: $F_{1,66}$ = 1.89, p = .174), coefficient of variation (occipital cortex: $F_{1,73}$ = 0.73, p = .395;

pericalcarine region: $F_{1,73}$ = 0.03, p = .853), nor ITPL value (occipital cortex: $F_{1,74}$ = 0.65, p = .423; pericalcarine region: $F_{1,74}$ = 0.34, p = .564).

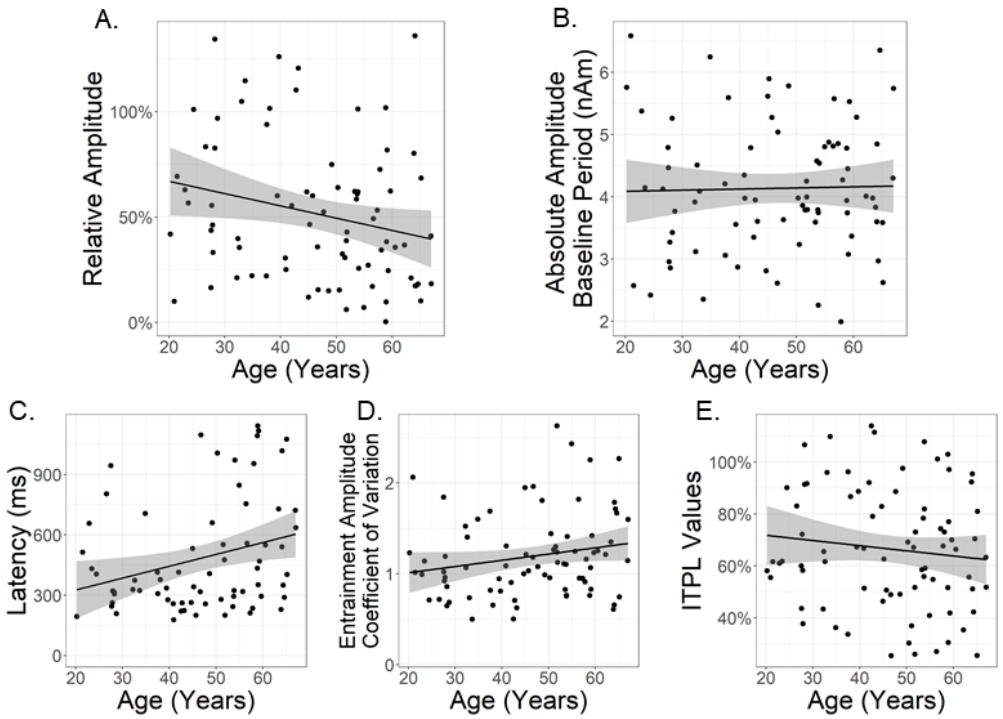

Figure 3. Relationships between age and several neural indices of the entrainment response.

(A) Entrainment response amplitude, (B) Amplitude of spontaneous activity during the baseline period, (C) entrainment response latency, (D) intertrial amplitude consistency (i.e., coefficient of variation), and (E) intertrial phase consistency (i.e., intertrial phase locking; ITPL) are shown as a function of participant age. Lines of linear best-fit, 95% CI (i.e., shaded area).

Next, we wanted to investigate the relationship between response latency and mean entrainment response amplitude, as well as whether latency modulates the relationship between participant age and mean entrainment response. To this end, we regressed the mean entrainment response amplitude onto latency and found that participants with later response latencies (i.e., took longer to entrain to the flickering stimuli) also tended to have weaker mean entrainment responses ($F_{1,69}$ = 11.60, p = .001). To investigate whether latency mediated the relationship between age and mean entrainment amplitude, a mediation analysis was conducted (115), with indirect effects estimated using bootstrapping (113). Our results (Figure 4 and Table 1) indicated a full

mediation of the relationship between age and mean entrainment amplitude by latency, which survived bootstrapping of 5,000 samples (95% CI: -.0051 through -.0004). Importantly, these results suggest participant response latency drives the effects of age on the strength of visual entrainment. Further, as with all analyses, the indirect effect of age on mean entrainment amplitude through latency remained significant when controlling for visual cortical thickness.

Model	*b*	*SE*	*t*	β	*F*	R^2	95% CI
Simple regression of response latency on age							
Intercept	215.72	117.05	1.84		5.86*	.08	[-17.85, 449.28]
Age	5.81	2.40	2.42*	.282			[1.02, 10.61]
Simple regression of relative entrainment amplitude on age							
Intercept	0.85	0.144	5.90**		5.36*	.07	[0.56, 1.14]
Age	-0.01	0.01	-2.32*	-.270			[-0.01, -0.001]
Multiple regression of relative entrainment amplitude on age and response latency							
Intercept	0.94	0.14	6.68		7.08**	.17	[0.66, 1.22]
Latency	0.00	0.00	-2.87**	-.332			[-0.001, -0.0001]
Age	-0.01	0.00	-1.53	-.177			[-0.01, 0.001]

Table 1. Entrainment latency fully mediates the relationship between age and entrainment amplitude.

Mediation analysis underlying regressions showing full mediation of the relationship between age and relative entrainment amplitude through latency. *$p < .05$, **$p < .01$.

Finally, to further explore these changes in entrainment latency and amplitude as a function of healthy aging, permutation testing of the relative entrainment time series was performed using an initial *p*-value threshold of 0.05 and 10,000 permutations to build the null distribution. Interestingly, of the whole entrainment period (0 to 2500 ms), only the beginning (400 to 1800 ms) differed significantly as a function of age ($p < .05$, corrected). These permutation data provide further support for the idea that changes in the response latency with age may be driving decreases in the overall entrainment amplitudes of older individuals.

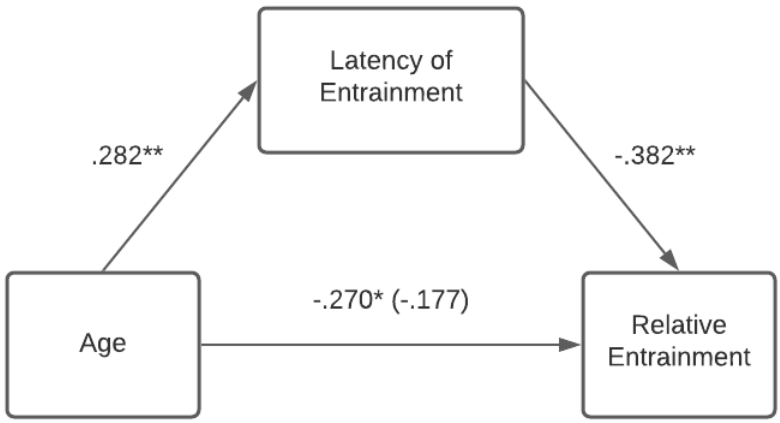

Figure 4. Mediation path diagram.

Mediation analysis revealed that the relationship between age and mean entrainment amplitude was fully mediated by the latency of the entrainment response. This analysis survived bootstrapping of 5,000 samples with confidence intervals of 95%. Standardized regression coefficients are displayed. Displayed statistical parameters were not significantly altered when occipital or pericalcarine cortical thickness values were included as nuisance covariates. *$p < .05$, **$p < .01$.

Discussion:

In the current study, we investigated the impact of healthy aging on the visual processing of flickering stimuli in the primary visual cortices while controlling for occipital cortical thickness. Using advanced source reconstruction and voxel time series analyses, we observed robust cortical entrainment at the frequency of stimulation (i.e., 15 Hz) and its harmonics. As expected, as a function of healthy aging, mean entrainment responses were found to decrease in amplitude, while the peak latency of entrainment responses were found to increase. Further, older individuals were found to have decreased cortical thickness across the entire brain and in the visual cortices. These data revealed that entrainment response latency fully mediated the relationship between age and entrainment amplitude, and that these age-related effects surrounded the calcarine fissure. Critically, these changes in visual entrainment response metrics as a function of age were independent of age-related visual cortical thinning. Below, the

implications of these novel findings on understanding the impact of healthy aging on visual processing are discussed.

Two common findings in the fMRI and electrode/sensor-level electrophysiologic literature investigating visual processing in healthy aging are decreased amplitude (66-69, 75-78) and increased latency (66, 68, 70-75) with increasing age. Our findings support these changes with increasing age predicting weaker visual entrainment and extended time required to fully entrain to the flickering stimulus, and add new anatomical detail on the cortical origins. Broadly speaking, little is known about the underlying cause of such decreased visual response amplitudes in older individuals. In line with the cortical thickness findings in the current study, Peiffer (77) showed significantly decreased visual response amplitudes even when controlling for visual cortical gray matter loss with increasing age. This research by Peiffer and colleagues (77), along with our results showing that visual cortical thinning in older adults is not associated with age-related alterations in visual responses, indicate that age-related changes in visual response properties stem from mechanisms other than the age-related cortical atrophy seen in older individuals. With regards to mechanisms for increased latency of visual responses with age, however, a fascinating MEG study by Price (74) demonstrated that prolonged latencies with increasing age could be largely explained by white matter loss in the optic radiations of participants, causing delays in signal transmission.

A secondary goal of the current study was to probe for neurophysiological response parameters that may underlie the decreased visual response amplitudes observed in healthy aging. To this end, we investigated inter-trial phase consistency using the ITPL metric and single trial amplitude using the coefficient of variation (CV), both of which have not been utilized in a healthy aging population. The use of ITPL provides information regarding trial-to-trial phase response consistency that is interpretationally distinct from the coefficient of variation computed on response

amplitude across trials. Specifically, ITPL tells us how consistently the phases of the neural signal are aligning from trial to trial (at the same time point) for each participant, while the CV is based on signal amplitude metrics and reflects how consistent the strength of the neural response is from trial to trial. Considering the well documented age-related changes to visual processing, we hypothesized that the consistency of visual responses would decrease with participant age, and thus be a major contributor to the overall decrease in mean amplitude. Interestingly, we observed no such changes in the consistency of the phase (i.e., ITPL) nor amplitude (i.e., CV), which supports the null hypothesis that these parameters do not play a significant role.

A key finding from our time series analyses indicated that older individuals reach their maximum entrainment amplitude much more slowly than their younger peers. This sort of change in response properties has been shown on a different time scale in fMRI visual processing studies, where older individuals were found to have hemodynamic response curves that were both flatter and more sustained than younger individuals (75, 80). Similarly, in the current study, visual entrainment response latency was found to predict the mean amplitude of entrainment such that participants who took longer to entrain had weaker overall responses. Thus, to further probe the relationship between age, visual response amplitude, and latency, we conducted a mediation analysis with latency as the mediator. Critically, we found that response latency fully mediated the relationship between age and visual response amplitude, indicating that older individuals may have weaker overall visual responses *because* they are taking longer to entrain the flickering stimuli. This view was fully supported by our permutation analysis of the time series, which showed that older individuals did not statistically differ from younger individuals during the later entrainment period. The fact that older individuals take longer to reach the same visual response amplitude as their younger counterparts is both novel and has important implications for the interpretation of electrophysiologic visual

paradigms. In the most common visual stimulation paradigms used in aging research, a stimulus is presented and removed quickly, causing a visual evoked potential. Comparably, entrainment tasks involve quickly flickering the stimulus over and over, which causes a sustained response. The results herein suggest that older participants may have significantly weaker initial visual responses that start to approximate those of their younger peers if the stimulus change is sustained and periodic. Thus, the literature's most common age-related finding in the visual domain may reflect only part of the story, as the decrease in response amplitude is likely paradigm specific.

A somewhat surprising finding was the lack of differences in spontaneous cortical activity as a function of age. Multiple studies have shown elevated spontaneous activity in the primary somatosensory cortices of older adults relative to younger adults (116) and in populations thought to exhibit accelerated aging such as those infected with HIV (117-121). Likewise, studies have shown elevated spontaneous activity in the primary motor cortices of healthy older relative to younger participants and demonstrated that such activity modulates behavioral performance and oscillatory responses in the same brain tissue (122-124). Thus, we were somewhat surprised that spontaneous activity did not differ as a function of age in the primary visual cortices. One possibility is that such aging effects are limited to the Rolandic region (i.e., extended sensorimotor strip), as we know of no studies showing elevated spontaneous activity with increasing age in the primary auditory or visual cortices. However, a second possibility is that the effect is specific to the idling rhythm of the cortical area, as the motor findings noted above were limited to the beta rhythm. While this is certainly possible, the elevated spontaneous activity reported in the somatosensory cortices of older adults has been limited to the gamma frequency range (116) and the somatosensory strip idles in the alpha band. The primary idling rhythm of the visual cortices is also alpha; thus, future studies should examine whether spontaneous alpha activity is elevated in the primary visual regions of

older adults. These studies would ideally involve a task that probes alpha frequency oscillations, as this would enable the impact of elevated spontaneous activity on cognitive and perceptual processing to be determined.

Before closing, it is important to note the limitations of this study. While our sample provided a wide range of ages (i.e., 20.22 to 67.00 years old), the top age was not as old as would have been ideal to cover the entire lifespan (i.e., ~ 80 years old). This is because some research has suggested that the visual declines associated with healthy aging do not significantly worsen until around age 60 (125-127). Second, the current study only utilized one frequency of stimulation. An interesting future direction would be to expand the frequency of stimulation to several frequencies, particularly those in the gamma band (i.e., > 30 Hz), in order to investigate frequency specific deficits in aging. Finally, despite collecting extensive neuropsychological data, our battery did not include specific assessments of visual processing and future studies of visual entrainment should expand their testing battery in this regard. Despite these limitations, we found that older adults exhibit weaker entrainment responses and that these deficits are largely attributable to older adults reaching peak entrainment much later than younger adults.

CHAPTER 2: HEALTHY AGING IS ASSOCIATED WITH ALTERED VISUAL GAMMA OSCILLATIONS

The material presented in this chapter is under review as Springer, Schantell, Okelberry, Willett, Johnson, and Wilson, 2023, Healthy Aging is Associated with Altered Visual Gamma Band Onset and Offset Responses

Introduction:

Previous work has demonstrated that the sharp increase in neural activity following the appearance of a visual stimulus (i.e., onset response), the weaker sustained activity when the stimulus remains in the visual field (i.e., sustained response), and the activity elicited by the removal of that same stimulus (i.e., offset response) are distinct processes (128-130). The functional relevance of each of these separate neural processes is readily apparent, with navigation through the environment being dependent on the ability to perceive visual stimuli appearing, remaining in view, and disappearing from the visual field. Though studies of the visual onset and sustained responses are quite common, research focusing on the visual offset response is scarce. This discrepancy may be due to the fact that the strength of the offset response is tightly linked to stimulus characteristics such as contrast, spatial frequency, and the total duration for which the stimulus is presented (131-133). Thus, the visual offset response is not present in all visual stimulation paradigms. Though visual processing is supported by differential oscillatory activity across several frequencies (i.e., theta, alpha, beta, and gamma), the only spectral window with onset, sustained, and offset responses to visual stimuli is gamma (134, 135).

Neural oscillations in the gamma band (~20-100 Hz) have been found in a variety of disparate brain regions (e.g., visual, auditory, motor, parietal; (91, 92, 136-139) and are associated with many unique cognitive functions (i.e., memory, attention, sensory processing; 140, 141, 142). Various early accounts proposed that gamma oscillations mediated the binding of separate stimulus features into a coherent visual precept (i.e.,

"binding by synchrony"; 143, 144). However, the broad involvement of gamma band activity across so many regions and during a wide variety of different cognitive functions has led others to suggest that gamma activity serves a less specific, more foundational role in cortical computations (e.g., synchronizing the output of excitatory neurons; 145, 146-148). In the occipital cortices, gamma oscillations have been shown to be crucial to various aspects of visual processing, including gestalt perception (149, 150), color processing (151), and the processing of grating stimuli (152). Further, these visual gamma responses have been shown to have high test-retest reliability (153, 154), with amplitude and peak frequency characteristics that are highly dependent on stimulus properties such as contrast and spatial frequency (155-157).

Beyond its role in typical brain functions, gamma band oscillations have been investigated in a variety of neuropsychiatric disorders. Specifically, alterations in gamma band activity have been demonstrated in individuals with schizophrenia (158, 159), autism (92, 160), and Alzheimer's disease (AD; 161, 162). Further, groundbreaking studies in mouse models of AD have shown that gamma band entrainment, either through direct interneuron stimulation or sensory entrainment, is effective in clearing disease-related pathological proteins (i.e., amyloid beta and hyperphosphorylated tau) while improving cognitive function (83, 84, 163). More recently, these findings have been extended to human participants with clinical trials demonstrating that this visual gamma band stimulation may slow the progression of AD-related functional degeneration (164). This is unfortunate, as a more thorough understanding of how healthy aging modulates visual gamma band responses is critical to distinguishing normal changes across the lifespan from those associated with pathological processes.

In this study, we utilized the high spatiotemporal precision of magnetoencephalography (MEG) to investigate age-related alterations in visual cortical oscillations. We were particularly interested in disentangling the unique gamma

oscillations in response to visual stimulus appearance (i.e., onset), the stimulus remaining on the screen (i.e., sustained), and the removal of the stimulus (i.e., offset). To elicit these responses, we used a visual grating paradigm that is known to evoke robust gamma oscillations. Based on the few previous studies of visual gamma oscillations in healthy older adults, we hypothesized that there would be significant age-related reductions in gamma band amplitude and inter-trial phase locking across all gamma responses.

Methods:

Participants

Eighty-seven adults with a mean age of 45.84 (SD = 13.20) years and a range of 20.22 to 66.98 years were selected for inclusion in this study. These participants were chosen from a larger-scale study of accelerated aging in people with HIV, with only the cognitively normal HIV-negative participants being included in this investigation of healthy aging. Of the 87 adults, 93% were right-handed, 12.6% were Black/African American, 7.0% were Asian, 74.7% were Caucasian, 4.6% were more than one race, and the remaining 1.2% preferred not to answer. This distribution corresponds closely to the racial demographics of the surrounding region. Notably, there was no effect of age on years of education (r_{85} = -.09, p = .379) and all included participants scored in the normal range on a neuropsychological testing battery that probed seven cognitive domains (i.e., processing speed, memory, learning, language, executive function, attention, and motor function). Exclusionary criteria included any medical illness affecting CNS function (e.g., HIV/AIDS, Lupus, etc.), any neurological or psychiatric disorder, cognitive impairment, history of head trauma, current substance use disorders, and the MEG laboratory's standard exclusionary criteria (e.g., ferromagnetic implants). The

Institutional Review Board reviewed and approved this investigation. Each participant provided written informed consent following a detailed description of the study.

Experimental Paradigm

Participants were shown a small, centrally located red fixation square on a grey background. A series of vertical, stationary, square-wave gratings (3 cycles per degree) appeared on the screen for 500 ms, before disappearing and leaving only the fixation square (Figure 5). The interval between the offset of the grating on one trial and the onset of the grating in the next trial randomly varied between 2000 and 2500 ms. Each participant completed a total of 120 trials, for a total run time of about 5.5 minutes.

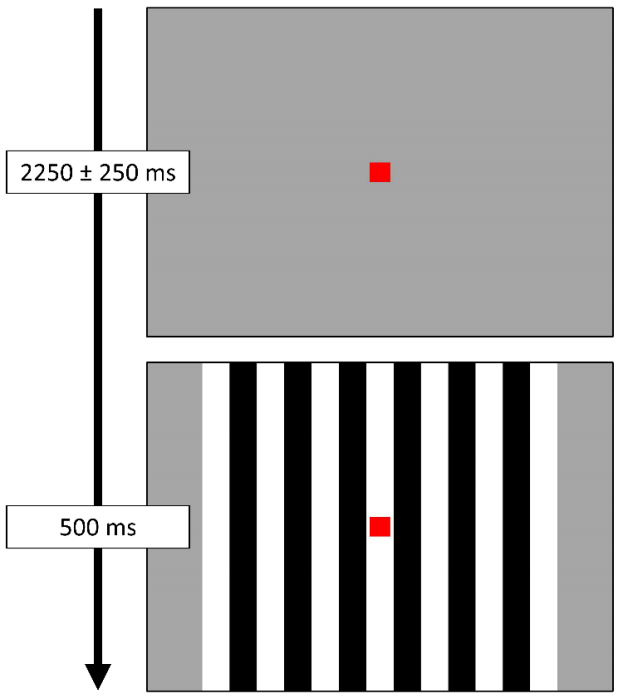

Figure 5. Visual grating task paradigm.

Participants were instructed to fixate on a red square presented centrally. Following the fixation period, a series of visual gratings appeared around the red square for 500 ms. Each participant completed 120 total trials.

MEG Data Acquisition

All recordings were conducted in a magnetically-shielded room with active shielding engaged. Neuromagnetic responses were sampled continuously at 1 kHz, with an acquisition bandwidth of 0.1-330 Hz, using a MEGIN MEG system with 306 magnetic sensors (MEGIN, Helsinki, Finland). During data acquisition, participants were monitored via real-time audio-visual feeds from inside the shielded room. Subject-wise MEG data

were corrected for head motion and subjected to external noise reduction using signal space separation with a temporal extension (97).

Structural MRI Processing and MEG Coregistration

Preceding MEG measurement, four head position indicator (HPI) coils were attached to the participant's head and localized, together with three fiducial points and at least 100 scalp surface points, with a 3D digitizer (Fastrak 3SF0002, Polhemus Navigator Sciences, Cohshester, VT, USA). Once in the MEG, electrical currents with unique frequencies (e.g., 322 Hz) were fed into each of the HPI coils. These HPI coil currents induced measurable magnetic fields, allowing the position of the HPI coils to be tracked relative to the MEG sensors throughout the recording. Since HPI coil locations were also known in head coordinates, all MEG measurements could be transformed into a common coordinate system. With this coordinate system, participant-wise MEG data were coregistered with high-resolution structural T1-weighted MRI data prior to source reconstruction using Brain Electrical Source Analysis (BESA) MRI (Version 2.0, BESA GmbH, Gräfelfing, Germany). Structural MRI data were transformed into standardized space and aligned parallel to the anterior and posterior commissures. Following source analysis, each participant's MEG functional images were also transformed into standardized space using the same transform and spatially resampled.

MEG Preprocessing, Time-Frequency Transformation, and Sensor-Level Statistics

Blink and cardiac artifacts were removed from the raw data using signal-space projection, and this correction was accounted for during source analysis (165). The continuous magnetic time series was divided into 1800 ms epochs, with the baseline period being defined as the -350 ms to -50 ms period prior to stimulus presentation (i.e., defined as 0 ms). Subsequently, epochs containing artifacts were removed based on a fixed threshold method, supplemented with visual inspection. Briefly, the amplitude and gradient distributions across all trials were determined per participant, and those trials

containing the highest amplitude and/or gradient values relative to this distribution were rejected based on participant-specific thresholds. This approach was employed to minimize the impact of individual differences in sensor proximity to the brain and overall head size, which strongly affect MEG signal amplitude. Importantly, there were no age-related changes in either the amplitude (r_{85} = .01, p = .923) or gradient (r_{85} = .06, p = .579) thresholds used for artifact rejection. Artifact-free epochs were then transformed into the time-frequency domain using complex demodulation (99, 166, 167). Lower frequency responses (i.e., theta, alpha, and beta) were transformed into the time-frequency domain using a resolution of 1 Hz 50 ms, while higher frequency responses (i.e., gamma) were transformed using a resolution of 2 Hz 25 ms. Following time-frequency transformation, spectral power estimates per sensor were averaged across trials to generate plots of mean spectral density per sensor. These sensor-level data were then normalized to the baseline power within each frequency bin, which was calculated as the mean power for that frequency bin during the baseline time period (i.e., -350 to -50 ms; Figure 6A).

The significant time-frequency windows used for source imaging were determined by statistical analysis of the sensor-level spectrograms across the entire array of gradiometers. Briefly, each pixel was initially evaluated using a mass univariate approach based on the general linear model, followed by cluster-based permutation testing to address the problem of multiple comparisons (100, 101). Specifically, a two-stage procedure was utilized to minimize false positive results while maintaining sensitivity. The first stage consisted of performing paired-sample t-tests against baseline on each pixel per spectrogram and thresholding the output spectrograms at $p < .05$ to define time-frequency bins containing potentially significant oscillatory deviations from baseline. Bins surviving this threshold (at $p < .05$) were clustered with temporally and/or spectrally neighboring bins that also survived, and cluster values were derived by

summing all t-values within each cluster. In stage two, nonparametric permutation testing was used to derive a distribution of cluster-values and the significance level of the cluster(s) from stage one were tested directly using this permuted distribution, which was the result of 10,000 permutations. Based on this permutation analysis, only the time-frequency windows that contained significant oscillatory deviations from baseline at the $p < .001$, corrected, threshold across all participants were subjected to source imaging.

MEG Source Imaging and Statistics

Cortical networks were imaged through a time-frequency resolved extension of the linearly constrained minimum variance (LCMV) vector beamformer (102-104). The subject-wise images were derived from the cross spectral densities of all combinations of MEG gradiometers averaged over the time-frequency range of interest, and the solution of the forward problem for each location on a grid specified by input voxel space. In principle, the beamformer operator generates a spatial filter for each grid point that passes signals without attenuation from the given neural region, while suppressing activity in all other brain areas. The filter properties arise from the forward solution (i.e., lead field matrix) for each location on a volumetric grid specified by input voxel space, and from the MEG data covariance matrix (i.e., cross spectral density matrix). Basically, for each voxel, a set of beamformer weights is determined, which amounts to each MEG sensor being allocated a sensitivity weighting for activity in the particular voxel. Following convention, the source power in these images was normalized per participant using a pre-stimulus period (i.e., baseline) of equal duration and bandwidth (105). Such images are typically referred to as pseudo-t maps, with units (pseudo-t) that reflect noise-normalized power differences (i.e., active vs. passive) per voxel. MEG pre-processing and imaging used the BESA software (version 7.1).

After imaging, average whole-brain maps were computed across all participants for the selected time-frequency windows. These 3D maps of brain activity were used to

assess the neuroanatomical basis of the significant oscillatory responses identified through the sensor-level analysis. Using these grand averaged (i.e. across all participants) whole-brain maps, we then extracted virtual sensors (i.e., voxel time series) for the peak voxel of each cluster. Specifically, we identified the voxel with the strongest response in the grand average image and computed virtual sensors for that location by applying the sensor weighting matrix derived from the forward solution to the preprocessed signal vector, which yielded a time series for the specific voxel in source space. These virtual sensor time series were then transformed into the time-frequency domain using the same complex demodulation procedure as the sensor-level time-frequency decomposition. From these time-frequency virtual sensor data, the envelope of spectral power was computed for the frequency range used in each beamforming analysis (i.e., theta: 4-7 Hz, alpha: 8-12 Hz, beta: 14-20 Hz, gamma onset: 30-58 Hz, gamma sustained: 30-58 Hz, and gamma offset: 22-58 Hz). Estimates of the baseline-relative response amplitudes were derived by averaging across the time window used for beamforming in each frequency (i.e. theta: 0-250 ms, alpha: 200-500 ms, beta: 200-500 ms, gamma onset: 25-175 ms, gamma sustained: 200-500 ms, and gamma offset: 525-675 ms). Additionally, using these same peak voxel time series data, the envelope of spectral inter-trial phase locking (ITPL) was computed for the time-frequency range used in the beamforming analysis per participant. Bilateral occipital responses were averaged across hemisphere. To reduce the impact of outliers on statistical analyses, participants with values 3.0 SDs above or below their respective group mean were excluded for each analysis.

Statistical Analyses and Software

All statistical analyses were performed using *JASP* (168), and data plots were generated using *ggplot2* (111). Correlations and multiple regressions were used to model age-related changes in neural activity per response. Single

component responses (i.e., theta, alpha, beta, and sustained gamma) were separately correlated with age. Considering the strong relationship between the gamma onset and offset responses (r_{84} = .68, p < .001), age-related modeling of each of these responses controlled for the other gamma band response. Similarly, gamma onset and offset inter-trial phase locking (ITPL) values were strongly correlated (r_{85} = .73, p < .001); thus, age-related modeling of the ITPL of each of these responses controlled for the other gamma band ITPL estimate. To investigate the effect of age on the relationship between gamma onset amplitude and gamma offset amplitude, the interaction between age and gamma onset amplitude on gamma offset amplitude was modeled using multiple regression. This interaction was probed using a simple slopes analysis, with the slope values set to the recommended value of ± 1 SD (169). Finally, the relationship between gamma onset and offset amplitude and cognitive function was modeled using correlation analyses. Considering the relationship between age and the amplitude of the gamma responses, as well as the fact that the neuropsychological domains were corrected for age, the effect of age was removed from the gamma amplitude values in these neurobehavioral models. Finally, the gamma spectral windows differed for the onset (30-58 Hz) and offset (22-58 Hz) responses. To ensure these differences in bandwidth were not driving any of our results, all analyses were recomputed with the shared frequency range (i.e., 30-58 Hz) and none of the significant results changed.

Results:

MEG Sensor-level Analysis

Sensor-level time-frequency analysis across all participants revealed significant clusters (p < .001, corrected) of theta, alpha, beta, and gamma oscillatory activity (Figure 6A). Theta band activity sharply increased immediately following stimulus presentation and dissipated about 250 ms later (i.e., 4-7 Hz, 0-250 ms; p < .001, corrected).

Temporally overlapping decreases in alpha (8-12 Hz, 200-500 ms) and beta (14-20 Hz, 200-500 ms) activity began about 200 ms after stimulus onset and lasted until stimulus removal (i.e., 500 ms; both *p*s < .001, corrected). Finally, broadband increases in gamma band activity were observed following stimulus onset (30-58 Hz, 25-175 ms), while the stimulus remained on the screen (30-58 Hz, 200-500 ms), and following stimulus offset (22-58 Hz, 525-675 ms; all *p*s < .001).

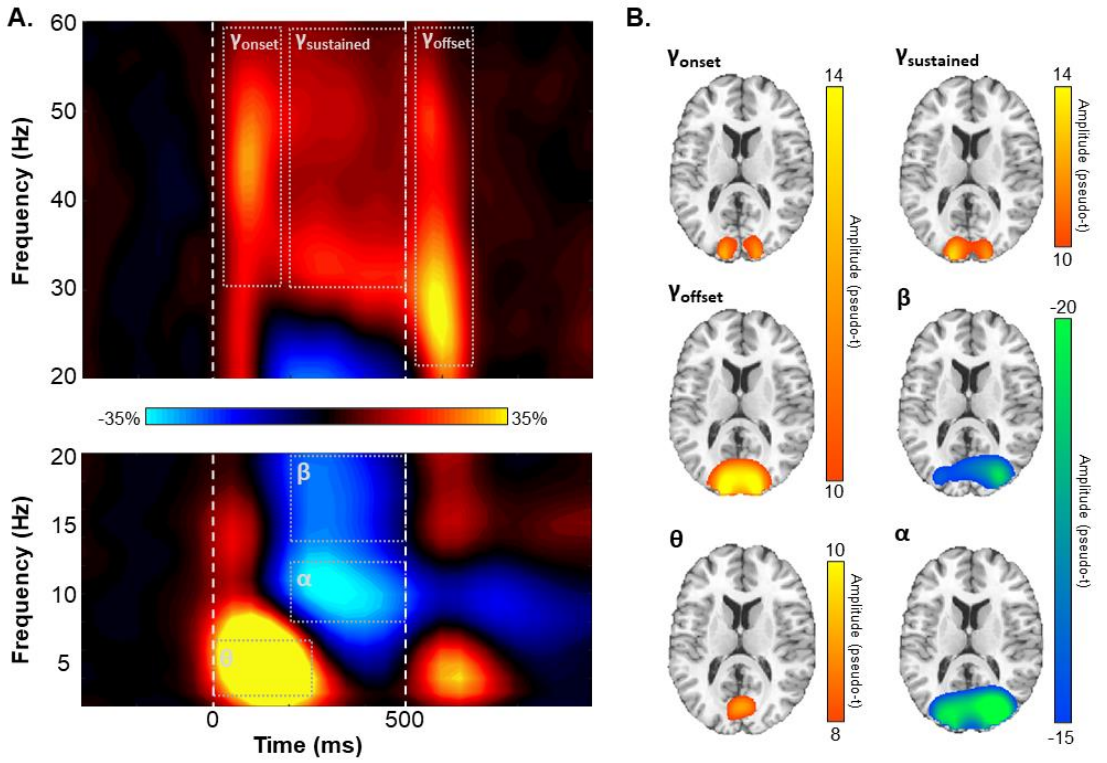

Figure 6. Sensor- and source-level activity during visual grating stimulation

A. Grand-averaged time-frequency spectrograms from a sensor near parieto-occipital areas (MEG2312), with time (ms) shown on the x-axis and frequency (Hz) on the y-axis. The vertical, dashed white lines denote stimulus onset (0 ms) and offset (500 ms). The colored scale bar between the spectrograms indicates the percentage power change relative to the baseline period (-350 to -50 ms). Significant time-frequency deviations from baseline were identified by cluster-based permutation analysis (see Methods section) and are highlighted using grey dot boundaries. B. Grand-averaged beamformer images across all participants for each time-frequency response. Colored scale bars for each beamformer image denote response amplitude in pseudo-*t* units.

Cortical-level and Time Series Analysis

To determine the cortical areas generating these significant sensor-level oscillatory responses, we imaged each window using a time- and frequency-resolved

beamformer. The resulting whole-brain maps per participant and response were then averaged across all individuals to determine the cortical origins of each oscillatory response (Figure 6B). Stronger increases in theta activity were observed in the calcarine fissure immediately following stimulus presentation (i.e., 0-250 ms). In contrast, strong decreases in alpha and beta activity were observed from about 200 to 500 ms in the lateral occipital cortices. Finally, bilateral primary visual gamma band activity increased at stimulus onset (i.e., 25-175 ms), was sustained during stimulus processing (200-500 ms), and increased again at stimulus offset (i.e., 525-675 ms).

To quantify the temporal dynamics of each oscillatory response and evaluate age-related alterations in this neural activity, baseline-relative amplitude and inter-trial phase locking (ITPL) values were computed from virtual sensor time series extracted from the voxel with the greatest amplitude per oscillatory response. Note that the peak voxel was virtually the same (i.e., within one voxel) for all three gamma responses (i.e., onset, sustained, and offset). No age-related amplitude changes were detected for the theta (r_{84} = .16, p = .131), alpha (r_{84} = .02, p = .824), beta (r_{85} = -.13, p = .232), or the sustained gamma response (r_{84} = .06, p = .560). The same was true for the ITPL measures in the alpha (r_{84} = .0.17, p = .128), beta (r_{84} = .06, p = .588), and sustained gamma (r_{83} = -.11, p = .336) responses, though there was an age-related increase in theta band ITPL (r_{83} = .27, p = .012). In contrast, significant age-related *increases* in gamma onset amplitude ($F_{1,82}$ = 10.67, p = .002; Figure 7) and ITPL ($F_{1,84}$ = 4.02, p = .048; Figure 8), controlling for the same parameters in the gamma offset response (see Methods), were detected in the primary visual cortices. Conversely, significant age-related *decreases* in gamma offset amplitude ($F_{1,82}$ = 7.72, p = .007; Figure 7) and ITPL ($F_{1,84}$ = 5.43, p = .022; Figure 8), controlling for the onset parameters, were observed in the primary visual cortices.

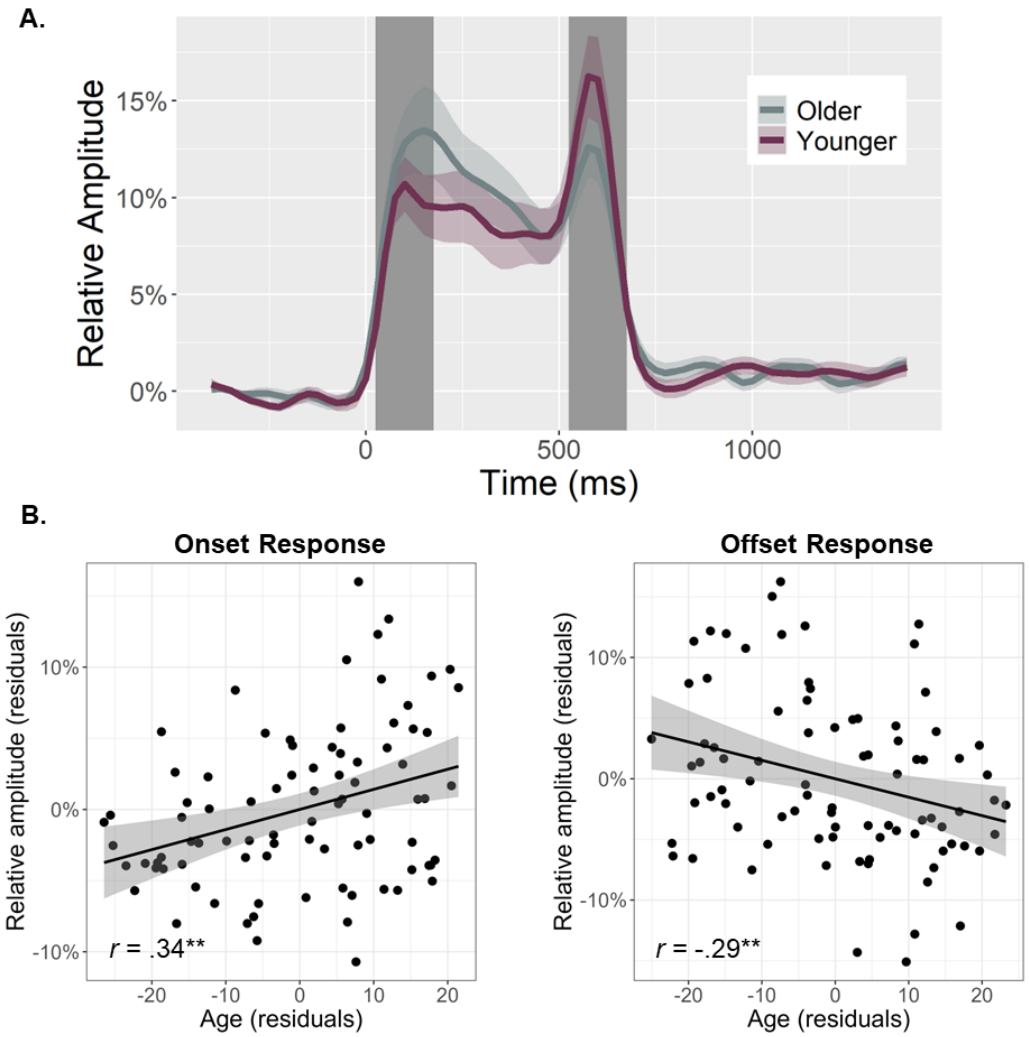

Figure 7. Primary visual gamma amplitude responses and age-related changes in these responses.

A. From the peak voxel showing the strongest gamma neural response, time series were extracted to evaluate changes in response amplitudes as a function of healthy aging during the time windows identified through sensor-level analysis (i.e., onset: 25-175 ms, offset: 525-675 ms; shaded area). The sustained response is not shaded as it was not related to age. Note that all statistics treated age as a continuous variable, but for the sake of visualization, participants have been dichotomized in this figure using a 0.5 SD from the mean cutoff. B. Scatterplots represent the average onset (left) and offset (right) response amplitude during each respective response time window (i.e., shaded area in A), as a function of age. Lines of linear best-fit and 95% CI (shaded areas in B) are shown. Given the high correlation between onset and offset gamma responses within each participant, the values plotted in (B) are corrected for the other response. $^{**}p < .01$

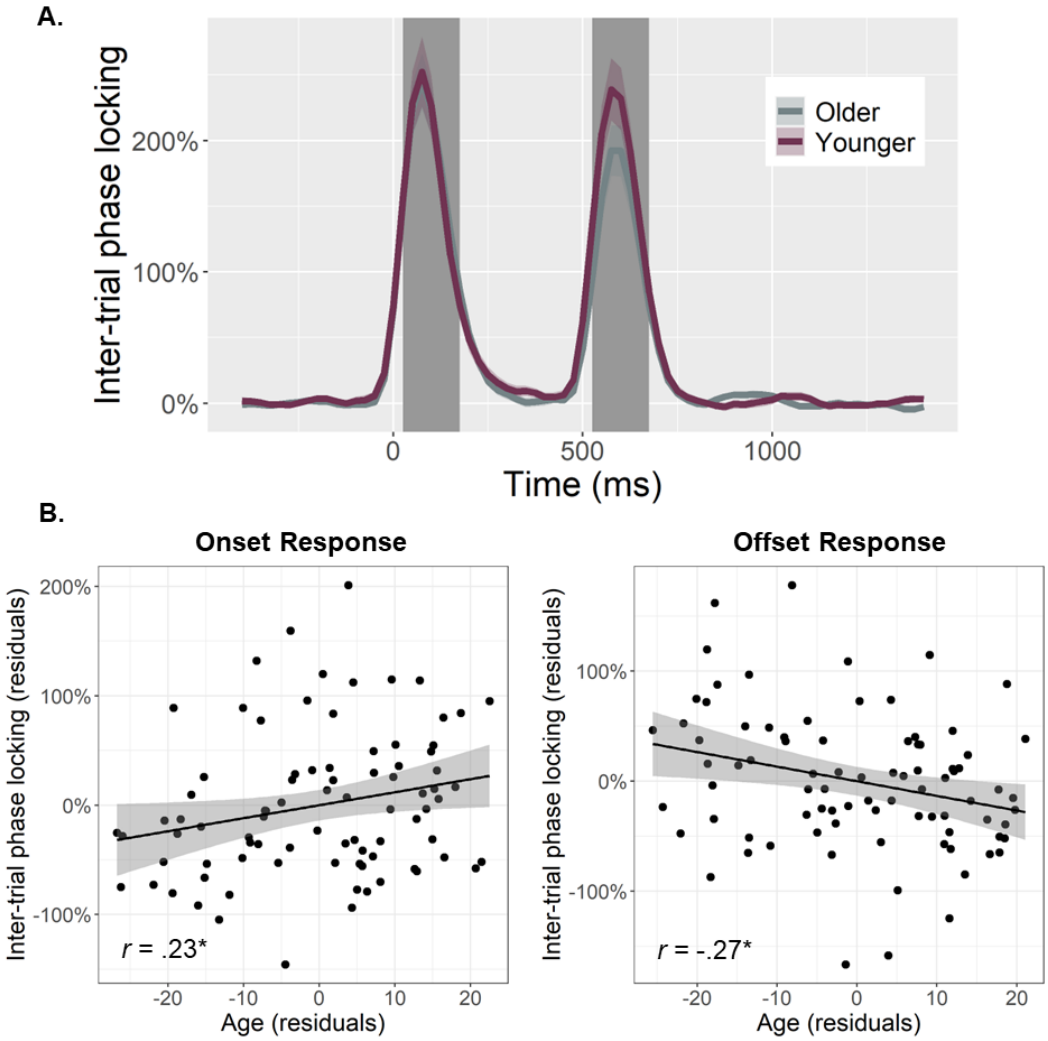

Figure 8. Inter-trial phase locking (ITPL) of visual gamma responses and age-related changes in ITPL.

A. Time series were extracted from the peak voxel based on response amplitude and used to compute ITPL values, which were examined as a function of healthy aging during the time windows identified through the sensor-level analysis (i.e., onset: 25-175 ms, offset: 525-675 ms; shaded area). The sustained response is not shaded as the ITPL value of this response was not related to age. Note that all statistics treated age as a continuous variable, but for the sake of visualization, participants have been dichotomized in this figure using a 0.5 SD from the mean cutoff. B. Scatterplots represent the average ITPL values for the onset (left) and offset (right) responses during each respective time window (i.e., shaded area in A), as a function of age. Lines of best linear fit and 95% CI (shaded areas in B) are shown. Given the high correlation between onset and offset gamma responses within each participant, the values plotted in (B) are corrected for the other response. *p < .05

Considering the strong relationship between gamma onset and offset amplitudes (r_{84} = .68, p < .001), we next investigated if this relationship was altered by age. To this end, we regressed gamma offset amplitude onto gamma onset amplitude with age as a

moderator and found a significant interaction between age and gamma offset amplitude ($F_{1,81}$ = 9.24, p = .003; Figure 9). Specifically, we found that as age increased, the strength of the relationship between gamma onset and offset amplitude decreased. This same age moderation was not found on the relationship between gamma onset and offset ITPL values ($F_{1,83}$ = 1.19, p = .194).

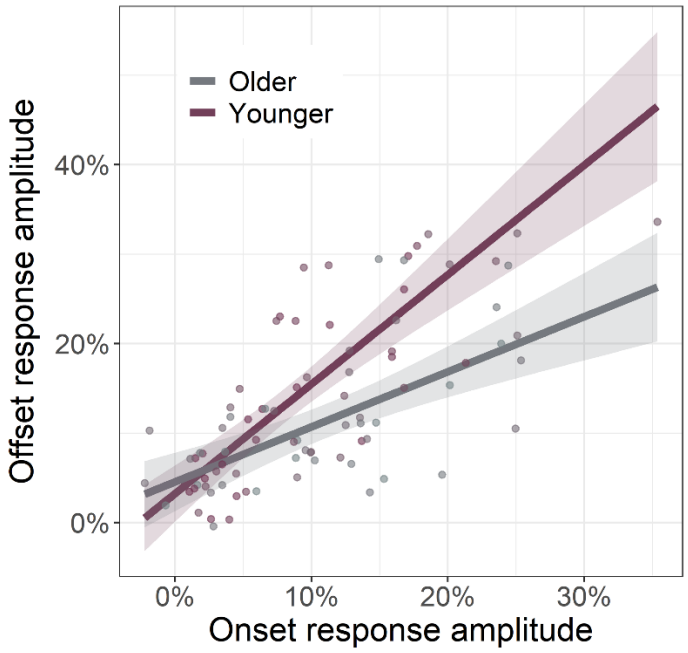

Figure 9. Relationship between gamma onset and offset response amplitude is moderated by age.

Across all participants, as the strength of gamma onset response amplitude increased, as did the strength of the gamma offset response amplitude. This gamma band onset-offset relationship was moderated by age, such that younger individuals had a stronger onset-offset relationship compared to older individuals. Since age was a continuous moderator, the interaction plot is modeled using simple slopes analysis (55), with age set to +1 SD from the mean (59.04 years old; Older) and -1 SD from the mean (32.64 years old; Younger), as is described in the Statistical Analysis section. Lines of linear best-fit and 95% CI (i.e., shaded area).

Lastly, we investigated the relationship between cognitive performance and visual gamma amplitude. We found a significant positive relationship between gamma offset amplitude and processing speed ($F_{1,81}$ = 6.08, p = .016; Figure 10). This same relationship did not exist between gamma onset amplitude and processing speed ($F_{1,79}$ =

2.05, p = .157). Further, neither gamma onset nor offset responses were significantly related to any of the other neuropsychological domains (ps > .05).

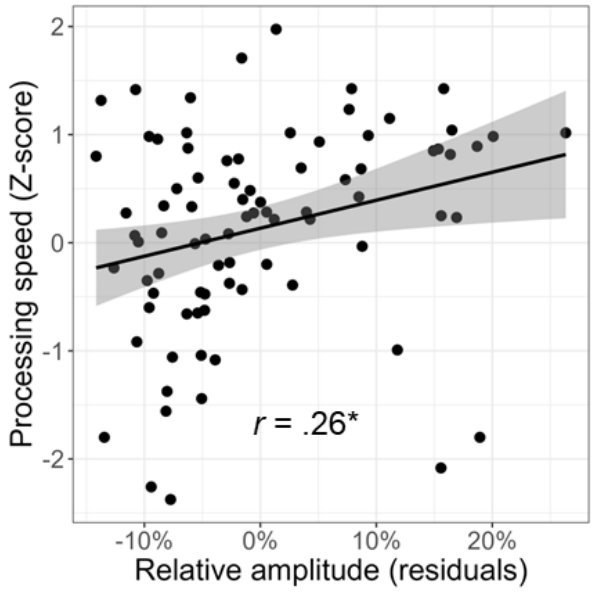

Figure 10. Relationship between processing speed and gamma offset response amplitude.

Across all participants, the strength of the gamma offset response was positively correlated with processing speed. Line of best linear fit and 95% CI (i.e., shaded area) are shown. *p < .05

Discussion:

Herein, we examined whether healthy aging modulates the oscillatory activity serving visual processing using MEG-based source reconstruction and voxel time series analyses. We found no significant age-related changes in occipital theta, alpha, beta, or sustained gamma responses. Our primary results indicated differential alterations in gamma onset and offset responses as a function of healthy aging. Specifically, we found that gamma *onset* amplitude and ITPL increased as a function of healthy aging. Conversely, gamma *offset* amplitude and ITPL decreased with increasing age. Further, gamma offset amplitude was found to positively predict participant processing speed. Finally, these data demonstrated that age moderates the relationship between gamma onset and offset amplitude. Specifically, younger adults exhibited a strong positive

relationship between gamma onset/offset amplitude, which was significantly diminished with increasing age. Below, we explore the implications of these novel findings for understanding the impact of healthy aging on visual processing.

The observed responses in the occipital cortices were in broad agreement with previous research on the oscillatory activity underlying visual processing. The theta activity observed at stimulus onset in the calcarine fissure is commonly elicited in studies of visually evoked potentials and has been widely implicated in the initial encoding of visual stimuli (148, 170). The suppression of alpha and beta band activity in the lateral occipital regions has been shown to represent active visual processing in higher-order visual areas (35, 141, 171-173). We found no age-related alterations in occipital theta, alpha, or beta band oscillations, with the exception of an age-related increase in the ITPL value of the theta response. This suggests that the phase of the theta response is more consistent per unit time in older compared to younger participants. The significance of this finding for visual processes is not entirely clear and should be a focus of future work. As has been previously shown, visual gamma band activity can be subdivided into several different types of responses. The visual gamma onset and offset responses are highly phase-locked (i.e., evoked) to the appearance and disappearance of a visual stimulus, while the sustained gamma response, between onset and offset, is typically not phase-locked across trials (i.e., induced; 134, 147, 157, 174, 175, 176). An exception to the phase-locked aspect can be seen in visual entrainment tasks, where the sustained response is tightly locked to the oscillating stimulus (177-181). Previous work by Muthukumaraswamy and colleagues (63) demonstrated that evoked visual gamma activity was highly consistent across recording sessions, while induced visual gamma activity showed large inter-individual variability in gamma band peak frequency, bandwidth, and amplitude. Source imaging demonstrated that the cortical distribution of both the visual onset and offset responses were virtually identical, with both responses

having the same peak in each hemisphere. This is in agreement with previous analyses showing that the onset and offset responses had similar scalp distributions (128, 182), which we further extend here by demonstrating that the sustained gamma response also originates from the same occipital cortical location as the evoked gamma onset and offset responses.

Our most striking findings were the age-related increases in the visual gamma onset response and decreases in the subsequent offset response, with no age-related changes in the sustained gamma oscillatory response. Interestingly, these age-related changes in gamma band amplitudes were mirrored by similar changes in ITPL, with there being stronger phase-locking to stimulus onset and weaker phase-locking to stimulus offset as a function of age. Further, we found that gamma onset and offset response amplitudes were positively correlated with one another, but that this positive relationship became weaker as a function of age. This onset-offset relationship presumably reflects the fact that stimuli which elicit stronger onset responses require stronger offset responses to “clear” the visual cortex once the visual stimulus has been removed. This hypothesis is indirectly supported by previous research which has demonstrated that onset and offset response amplitudes both scale with changes in the same visual stimulus properties (e.g., stimulus size, luminance, spatial frequency; 182, 183). The visual gamma onset response has been associated with the initial encoding of visual stimuli (152, 184-186); thus, our findings of age-related increases in this response likely indicates more effortful early processing of visual information. Interpretation of the weaker offset response with increasing age is more difficult considering the lack of previous research on visual offset responses. However, we believe that the decrease in offset response amplitude may relate to the observation that older individuals have longer visual persistence (187-190).

Visual persistence is the phenomenon in which an individual briefly continues to perceive a visual stimulus after that stimulus has been removed from the visual field. Longer visual persistence leads to slower overall sensory processing, as it takes these individuals longer to “recover” from one stimulus and to prepare to encode the next one (190-192). Supporting our hypothesis that the gamma offset response is related to visual persistence and thus sensory processing speed, we found a strong positive association between the amplitude of the gamma offset response and processing speed. This brain-behavior relationship was specific to the offset response, with there being no relationship between the onset response and processing speed. Similarly, it has been suggested that the longer visual persistence in older individuals may be related to deficits in inhibitory processing (187). This aligns with our findings of decreased gamma offset activity, as the generation of gamma oscillations has been repeatedly linked to the activity of GABAergic inhibitory interneurons (193, 194). Overall, our findings indicate that visual gamma oscillations, particularly the offset response, are useful metrics for probing age-related changes in visual processing and how these changes affect cognitive function.

Before closing, it is important to acknowledge several limitations of the current work. First, we used a spatial gratings stimulus; while this is one of the most widely used paradigms in basic visual research, our age-related findings may not generalize to all visual input. Another limitation is the cross-sectional nature of our study and future work in this area should consider longitudinal designs. Nonetheless, taken together, we found that gamma band cortical activity increased following both the appearance of a sinusoidal grating stimulus (i.e., onset) and when that stimulus was removed (i.e., offset). However, the amplitude and ITPL of these gamma band oscillations were differentially modulated by healthy aging, despite the fact that they originated from the same cortical locations. Specifically, older individuals had stronger gamma band visual onset responses, along with weaker visual offset responses. Critically, these age-related

decreases in the visual offset response predicted worse processing speed across all participants. Gaining a deeper understanding of these age-related changes in basic visual processing could hold major implications for designing specific interventions aimed at mitigating these visual changes, thus leading to better cognitive outcomes in older individuals.

CHAPTER 3: AGE-RELATED STRENGTHENING OF THE OSCILLATIONS SERVING VERBAL WORKING MEMORY PROCESSING

The material presented in this chapter was previously published in Springer, Okelberry, Willet, Johnson, Meehan, Schantell, Embury, Rempe, and Wilson, 2023, Age-related Alterations in the Oscillatory Dynamics serving Verbal Working Memory Processing, Aging

Introduction:

Working memory (WM) is a fundamental executive process which involves the storage, maintenance, and manipulation of relevant information. WM processes are generally grouped into three phases: information encoding, maintenance, and retrieval. The maintenance phase, which involves the rehearsal of the encoded information and the active inhibition of any new sensory stimuli, is the defining component which differentiates WM from other types of memory. Multiple studies have shown that WM processes are supported by a combination of neural spiking and oscillatory activity in the frontal and posterior cortices (140, 195-201). Historically, the neurophysiological underpinnings of WM function have been primarily investigated using functional MRI (fMRI). Such studies have revealed a left dominant, bilateral WM network with converging nodes in the dorsolateral prefrontal cortex (dlPFC), inferior frontal gyri, parieto-temporal cortices, and occipital regions (202-204). More recently, electrophysiological studies have helped illuminate the specific oscillatory dynamics underlying WM function. Specifically, theta band activity during WM performance has been associated with the encoding of visual stimuli in primary visual cortices and higher-order cognitive control in the prefrontal cortex (PFC) (201, 205-207). Similarly, alpha and beta band activity has been associated with higher-order visual processing in the posterior cortices and cognitive control in the PFC (35, 171, 207, 208).

Previous literature has demonstrated that WM processes are vulnerable to age-related decline (209-211), with these changes being particularly evident at higher cognitive loads (212-214). Across the adult lifespan, it has been shown that individuals

tend to recruit the same brain regions when performing WM tasks (35, 215). However, differential activation patterns become apparent when the cognitive load of the WM tasks is varied. For example, at lower cognitive loads, older individuals maintain WM performance comparable to younger individuals by recruiting more neural resources (i.e., stronger activations and/or more sites of activity) (215-217). Nevertheless, at higher cognitive loads, this neural compensation in older individuals faulters, resulting in behavioral decrements accompanied by weakened neural activity (212, 215, 218-220). This pattern of age-related overactivation, plateau, and subsequent underactivation is known as the compensation-related utilization of neural circuits hypothesis (CRUNCH) (20). The CRUNCH phenomenon has been most commonly observed in PFC regions (212, 215, 218, 221-223), which are thought to be responsible for exerting executive control over WM processes (203, 204). Further, these executive prefrontal areas have shown age-related differentiation in the lateralization of neural activity. Specifically, younger individuals consistently show stronger left hemispheric neural activity during WM performance, compared to a more bilateral pattern of activity in older adults (15, 16, 35, 215, 220, 221).

In addition to the plethora of past fMRI and positron-emission tomography (PET) work investigating age-related WM changes, more recent electrophysiologic work has been conducted to quantify the neural dynamics of these WM changes with age. One such study by Proskovec and colleagues (35) found that older adults had stronger alpha/beta oscillations (i.e., decreases in power relative to baseline), in right frontal regions during WM encoding and maintenance, and in the right superior temporal gyrus later in the maintenance phase. Conversely, it was shown that younger adults had stronger alpha/beta oscillations in the right parieto-temporal regions early in the encoding phase (35). Age-related changes in alpha activity during WM processing was later shown by Tran and associates (224), who demonstrated that older adults had lower

pre-trial alpha phase consistency, and that this lower phase consistency predicted lower WM task accuracy in older participants. Finally, event-related potential (ERP) analyses have revealed that, overall, older adults have reduced amplitudes in the fronto-central positivity (i.e., P200) and parietal positivity (i.e., P300) (225). However, when high- and low-performing older adults were separately analyzed, high-performing adults had stronger P200 and P300 amplitudes, more similar to younger adults (226). This interesting pattern of ERP results are in agreement with CRUNCH, with the high-performing older adults seemingly showing compensatory hyperactivation and the low-performing adults having reached a “resource ceiling” and decompensated.

Despite previous work characterizing age-related changes in WM, no previous studies have examined spectrally-specific age-related changes in neural oscillatory activity throughout all phases of WM (i.e., encoding, maintenance, and retrieval). Thus, in the current study we used the spatiotemporal precision of MEG to examine the effects of healthy aging on the spectrally-resolved neural oscillatory dynamics underlying all three phases of WM processing. We hypothesized that older adults would require stronger engagement of key left hemispheric frontal and parieto-occipital WM hubs. Additionally, we expected that prefrontal activity lateralization (i.e., stronger left hemispheric activity) during WM performance would diminish as a function of age, with older individuals tending to utilize a more bilaterally distributed WM network.

Methods:

Participants

Seventy-eight adults with a mean age of 45.10 (SD = 12.76) years were selected for inclusion in this study. The age range for males was 20.2 to 65.2 years and that for females was 21.4 to 62.2 years. These participants were chosen from a larger-scale study of accelerated aging in persons with HIV (227, 228), with only the HIV-negative

participants included in this investigation of healthy aging. Of the 78 adults, 95% were right-handed, 79% were male, 10% were African-American, 6% were Asian, 77% were Caucasian, 4% were more than one race, and the remaining 3% preferred not to answer. This distribution corresponds closely to the racial demographics of the surrounding region. Notably, there was no effect of age on years of education (r_{74} = -.073, p = .531) and all included participants scored in the normal range on a neuropsychological testing battery that probed seven cognitive domains (i.e., processing speed, memory, learning, language, executive function, attention, and motor function). Exclusionary criteria included any medical illness affecting CNS function (e.g., HIV/AIDS, Lupus, etc.), any neurological or psychiatric disorder, cognitive impairment, history of head trauma, current substance abuse, and the MEG laboratory's standard exclusionary criteria (e.g., ferromagnetic implants). The Institutional Review Board reviewed and approved this investigation. Each participant provided written informed consent following a detailed description of the study.

Experimental Paradigm

Participants were shown a centrally-presented fixation cross embedded in a 3×2 grid for 1.3 s (Figure 11). An array of six consonants then appeared at fixed locations within the grid for 2.0 s (i.e., encoding phase). Following the encoding phase, the letters disappeared and the empty grid remained on the screen for 3.0 s (i.e., maintenance phase). Finally, during the retrieval phase, a single probe consonant then appeared in the grid for 0.9 s, and the participant was instructed to respond via button press with their right index or middle finger as to whether the probe was in or out of the previous array of letters. A total of 128 trials were completed, equally split and pseudorandomized

between in- and out-of-set trials, for a total run time of about 15 min. This task has been utilized in several previous studies from our laboratory (35, 171, 229-232).

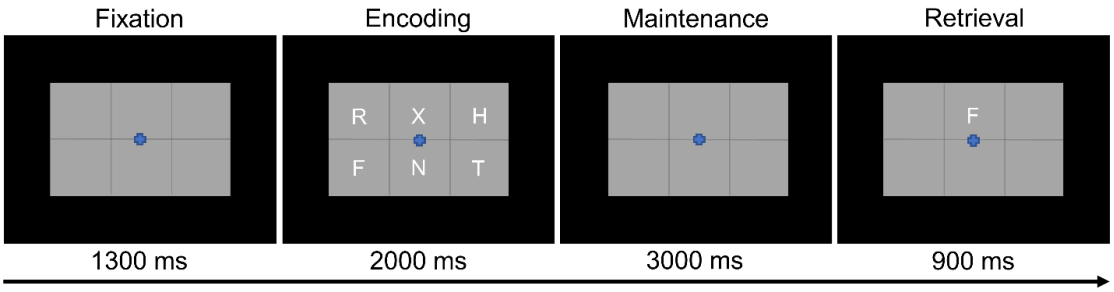

Figure 11. Modified Sternberg working memory paradigm.

Participants were required to encode and maintain six letter stimuli. During the retrieval stage, participants were then required to indicate whether the probe letter was or was not present in the initial six letter set.

MEG Data Acquisition

All recordings were conducted in a magnetically-shielded room with active shielding engaged. Neuromagnetic responses were sampled continuously at 1 kHz, with an acquisition bandwidth of 0.1-330 Hz, using a MEGIN Vectorview MEG system with 306 magnetic sensors (MEGIN, Helsinki, Finland). During data acquisition, participants were monitored via real-time audio-visual feeds from inside the shielded room. Subject-wise MEG data were corrected for head motion and subjected to external noise reduction using signal space separation with a temporal extension (97).

Structural MRI Processing and MEG Coregistration

Preceding MEG measurement, four head position indicator (HPI) coils were attached to the participant's head and localized, together with three fiducial points and at least 100 scalp surface points, with a 3D digitizer (Fastrak 3SF0002, Polhemus Navigator Sciences, Cohshester, VT, USA). Once in the MEG, electrical currents with

unique frequencies (e.g., 322 Hz) were fed into each of the HPI coils. These HPI coil currents induced measurable magnetic fields, allowing the position of the HPI coils to be activity tracked relative to the MEG sensors throughout the recording. Since HPI coil locations are known in head coordinates, all MEG measurements could be transformed into a common coordinate system. With this coordinate system, MEG data were coregistered with each individual's high-resolution structural T1-weighted MRI data prior to source reconstruction using Brain Electrical Source Analysis MRI (BESA MRI, Version 2.0, BESA GmbH, Gräfelfing, Germany). Individual structural MRI data for each participant was acquired using a Siemens Prisma 3T scanner (Siemens Medical Solutions) with a 64-channel head coil. An MP-RAGE sequence was utilized with the following parameters: TR: 2300 ms; TE = 2.98 ms; flip angle = 9°; FOV = 256 mm; slice thickness = 1.00 mm; voxel size = 1 × 1 × 1 mm. Structural MRI data were transformed into standardized space (i.e., Talairach space) and aligned parallel to the anterior and posterior commissures. Following source analysis, each participant's MEG functional images were also transformed into standardized space and spatially resampled.

MEG Preprocessing, Time-Frequency Transformation, and Sensor-Level Statistics

Blink and cardiac artifacts were removed from the raw data using an adaptive artifact correction method in which brain activity is selectively separated from artifactual activities (98). This adaptive artifact correction is accounted for during subsequent source analysis. The continuous magnetic time series was divided into 7200 ms epochs, with the baseline period being defined as the 400 ms prior to the encoding phase (i.e., -400 to 0 ms). Subsequently, epochs containing artifacts were removed based on a fixed threshold method, supplemented with visual inspection. Briefly, the amplitude and gradient distributions across all trials were determined per participant, and those trials containing the highest amplitude and/or gradient values relative to this distribution were rejected based on participant-specific thresholds. This approach was employed to

minimize the impact of individual differences in sensor proximity to the brain and overall head size, which strongly affect MEG signal amplitude. Importantly, there were no age-related changes in either the amplitude (r_{74} = -.182, p = .115) or gradient (r_{74} = -.135, p = .245) thresholds used for artifact rejection. Artifact-free epochs were then transformed into the time-frequency domain using complex demodulation (99, 166, 167), with a resolution of 1 Hz and 50 ms between 2 and 100 Hz. Following time-frequency transformation, spectral power estimates per sensor were averaged across trials to generate plots of mean spectral density per sensor. These sensor-level data were then normalized to the baseline power within each frequency bin, which was calculated as the mean power for that 1 Hz bin during the -400 to 0 ms time period.

The significant time-frequency windows used for source imaging were determined by statistical analysis of the sensor-level spectrograms across the entire array of gradiometers. Briefly, each pixel per spectrograms was initially evaluated using a mass univariate approach based on the general linear model, followed by cluster-based permutation testing to address the problem of multiple comparisons (100, 101). Specifically, a two-stage procedure was utilized to minimize false positive results while maintaining sensitivity. The first stage consisted of performing paired-sample t-tests against baseline on each pixel per spectrogram and thresholding the output spectrograms of t-values at $p < .05$ to define time-frequency bins containing potentially significant oscillatory deviations from baseline. Bins that survived thresholding (at $p < .05$) were clustered with temporally and/or spectrally neighboring bins that also survived, and cluster values were derived by summing all t-values within each cluster. In stage two, nonparametric permutation testing was used to derive a distribution of cluster-values and the significance level of the cluster(s) from stage one were tested directly using this permuted distribution, which was the result of 10,000 permutations. Based on this cluster-based permutation analysis, only the time-frequency windows that contained

significant oscillatory deviations from baseline at the $p < .001$, corrected, threshold across all participants were subjected to source imaging (i.e., beamforming).

MEG Source Imaging and Statistics

Cortical networks were imaged through a time-frequency-resolved extension of the linearly constrained minimum variance (LCMV) beamformer (102-104). The images were derived from the cross spectral densities of all combinations of MEG gradiometers averaged over the time-frequency range of interest, and the solution of the forward problem for each location on a grid specified by input voxel space. In principle, the beamformer operator generates a spatial filter for each grid point that passes signals without attenuation from a given neural region, while suppressing activity in all other brain areas. The filter properties arise from the forward solution (i.e., lead field matrix) for each location on a volumetric grid specified by input voxel space, and from the MEG cross spectral density matrix. Basically, for each voxel, a set of beamformer weights is determined, which amounts to each MEG sensor being allocated a sensitivity weighting for activity in the particular voxel. Following convention, the source power in these images was normalized per participant using a pre-stimulus period (i.e., baseline) of equal duration and bandwidth (105). Such images are typically referred to as pseudo-t maps, with units (pseudo-t) that reflect noise-normalized power differences (i.e., active vs. passive) per voxel. MEG pre-processing and imaging used BESA (version 7.0) software.

After imaging, average whole-brain maps were computed across all participants for the selected time-frequency windows. These 3D maps of brain activity were used to assess the neuroanatomical basis of the significant oscillatory responses identified through the sensor-level analysis. Finally, these source images were subjected to correlation analyses with age to investigate how the oscillatory processes underlying WM encoding, maintenance, and retrieval change as a function of age. To control for the

multiple comparisons inherent to whole-brain voxel-wise statistics, cluster-based permutation testing was again utilized (100, 101, 233). This whole-brain cluster-based permutation testing was virtually identical to the approach used for sensor-level statistics (see above), with the exception that the input data was voxel-level neural responses and we used a different statistical threshold following permutation testing (i.e., stage one threshold of $p < .001$; threshold of $p < .05$ following permutation testing for multiple comparisons correction).

Statistical Analyses

Statistical analyses were performed using custom *R* (110) and MATLAB (114) scripts. Correlation analyses were used to test for differences as a function of healthy aging in education, accuracy, reaction time, total correct trials, amplitude cutoffs, and gradient cutoffs. Permutation testing of the sensor-level spectrograms and whole-brain images was performed using BESA Statistics (Version 2.1, BESA GmbH, Gräfelfing, Germany). Correlation analyses were used to test for relationships between these age-related neural differences and cognitive function. Considering the relationship between age and these neural responses, as well as the fact that the neuropsychological domains were corrected for age, the effect of age was removed from the pseudo-t values in these neurobehavioral models. Finally, to reduce the impact of outliers on statistical analyses, participants with values 2.5 SDs above or below the group mean were excluded for each analysis.

Results:

Behavioral Results

Of the 78 participants that performed the verbal WM task, two were removed due to poor task performance (i.e., < 65% correct). While there was no effect of age on accuracy ($r_{74} = .012$, $p = .919$), there was an effect of age on reaction time ($r_{74} = .453$, p

< .001) such that older participants were slower than younger participants. Across all participants, the mean accuracy was 84.33% (SD = 7.04%) and the mean reaction time was 895.4 ms (SD = 193.06 ms).

Sensor-level analysis

Sensor-level time-frequency analysis across all participants revealed significant clusters ($p < .001$, corrected) of theta, alpha, and beta band oscillatory activity during the encoding, maintenance, and retrieval phases (Figure 12). During the encoding phase, theta band (3-6 Hz) activity sharply increased immediately following stimulus presentation (i.e., 0 ms), continued through the encoding phase, and slowly dissipated over the first 800 ms of the maintenance phase (i.e., 3-6 Hz, 0-2800 ms; $p < .001$, corrected). Additionally, decreases in alpha band (9-15 Hz) activity began around 200 ms after the onset of the encoding grid and were sustained throughout the encoding phase, terminating near the beginning of the maintenance phase (i.e., 9-15 Hz, 200-1800 ms; $p < .001$, corrected). During the maintenance phase, there was a significant cluster of increased alpha/beta activity in a slightly higher frequency band (12-17 Hz; 2500-2900 ms; $p < .001$, corrected). During the retrieval phase, an increase in theta activity followed retrieval probe presentation (3-6 Hz; 5000-5350 ms; $p < .001$, corrected). Finally, overlapping decreases in alpha (8-12 Hz; 5350-5750 ms) and beta (14-19 Hz; 5250-5650 ms) band activity were observed during the retrieval phase (both ps < .001, corrected).

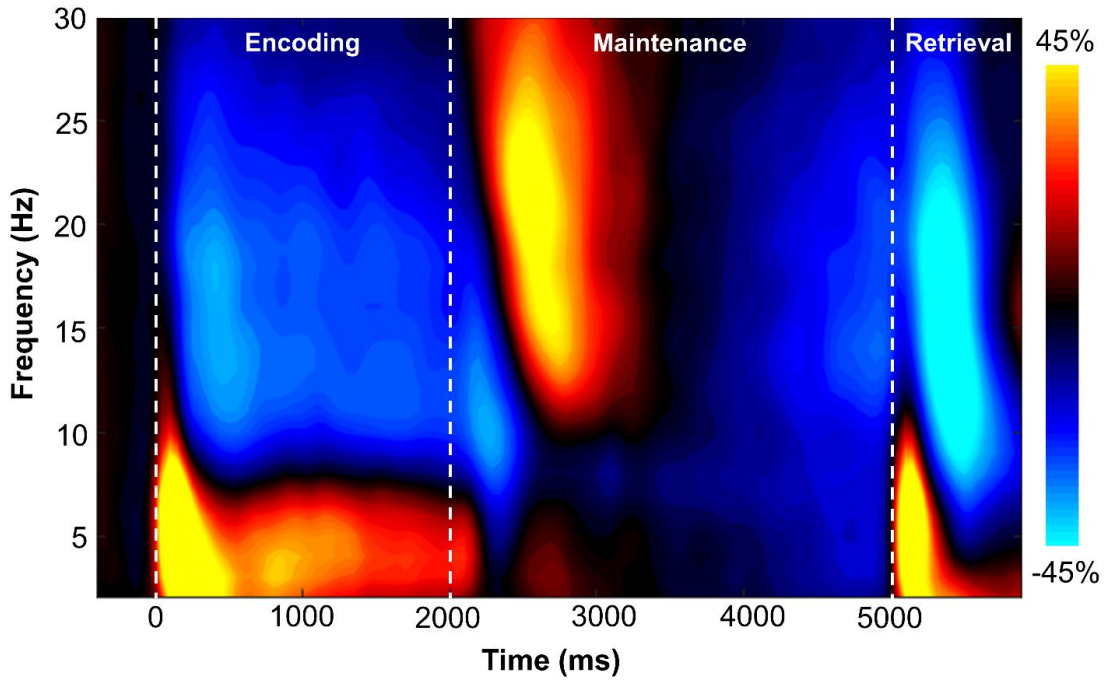

Figure 12. Sensor-level activity during verbal working memory task.

Grand-averaged time-frequency spectrogram from a sensor near parieto-occipital areas (MEG1922) with time (ms) shown on the x-axis and frequency (Hz) denoted on the y-axis. A color scale bar is shown to the right of the spectrogram which shows the percent power change relative to the baseline period (-400 to 0 ms).

Beamformer Analysis

In order to determine the neural regions involved in verbal WM, the aforementioned sensor-level time-frequency bins of interest for theta, alpha, and beta band oscillatory activity were imaged using a time-frequency-resolved beamformer. Considering that beamforming windows must be the same length as the baseline period (i.e., 400 ms), the oscillatory deviations from baseline were imaged in 400 ms increments or less. For the temporally extended oscillatory responses (i.e., those over 400 ms), participant-level image averaging was performed for each neural response as follows: theta encoding (3-6 Hz; 0-2000 ms), theta maintenance (3-6 Hz; 2000-2800 ms), and alpha encoding (9-15 Hz; 200-1800 ms). These whole-brain average maps per participant were then averaged across all individuals to allow for visualization of the

neural oscillations during the different WM phases (i.e., encoding, maintenance, and retrieval; Figure 13). These images revealed differential patterns of neural activity in the

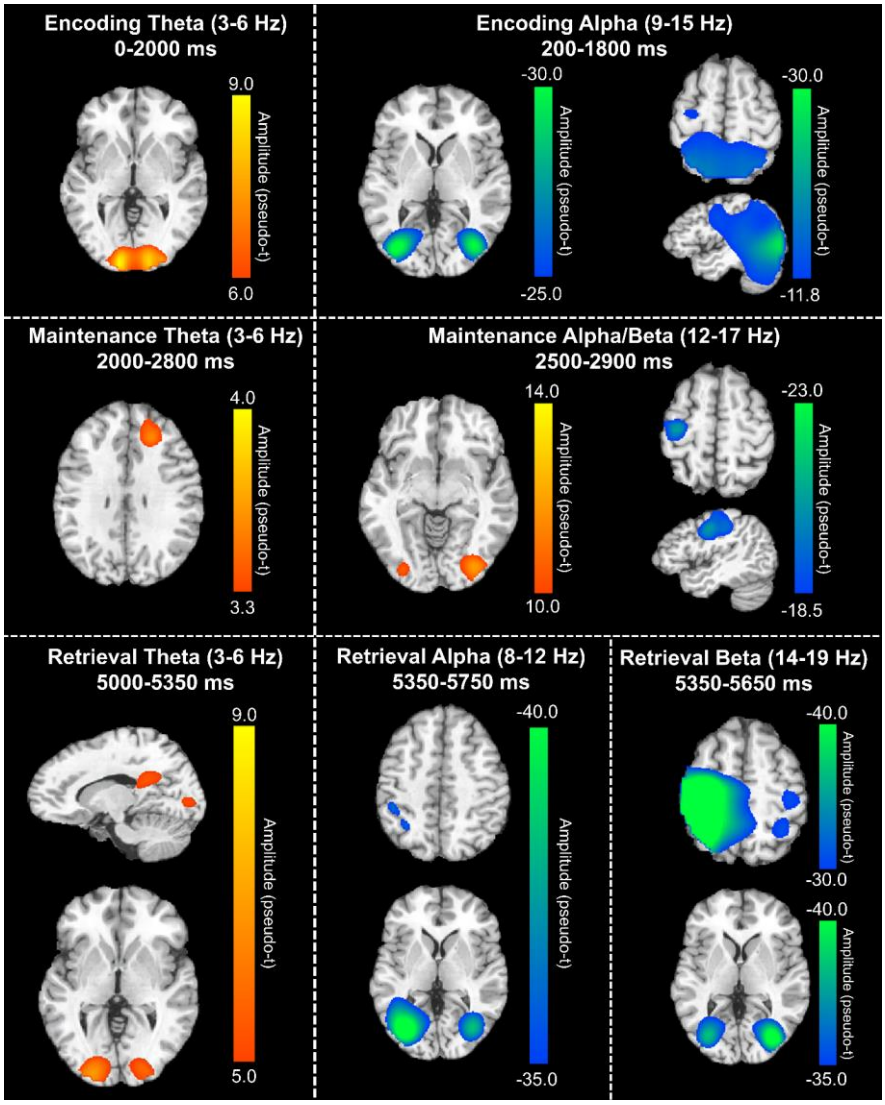

Figure 13. Source-level activity during verbal working memory task.

Grand-averaged beamformer images (pseudo-t) across all participants for theta (left) and alpha/beta (right) bands. During the encoding phase (top), there were increases in theta band amplitude relative to baseline in the primary visual cortex and decreases in alpha band activity (i.e., more negative relative to baseline) in the lateral occipital cortices, parietal cortices, and left hemisphere frontal cortex (including language areas). During the maintenance phase (middle), theta increases were limited to the right dlPFC and decreased alpha/beta activity in the left hemisphere frontal cortex (relative to baseline) was largely sustained. Additionally, a decrease in alpha/band activity relative to the baseline was observed in the lateral occipital cortices during the maintenance phase. During the retrieval phase (bottom), theta band activity increased in the right posterior cingulate gyrus and bilateral primary visual cortices, while alpha activity decreased (i.e., became more negative) in the lateral occipital cortices, left SMG, and left angular gyrus. Finally, decreased beta activity (i.e., more negative relative to baseline) in the bilateral primary motor cortices, lateral occipital cortices, and right superior parietal lobe was observed.

theta, alpha, and beta bands throughout all phases of WM performance. During the encoding phase, a strong increase in theta activity relative to the baseline was observed in the bilateral primary visual cortices, while decreased alpha activity (i.e., more negative relative to baseline) was observed in the lateral occipital cortices bilaterally, and left frontal cortex. During the maintenance phase, increased theta activity was observed in the right dorsolateral prefrontal cortex (dlPFC). Further, the decreased alpha/beta oscillations (i.e., more negative) observed in the frontal cortices during the encoding phase were sustained through the maintenance phase, along with decreased alpha activity in the lateral occipital cortices bilaterally. During the retrieval phase, theta band activity was shown to strongly increase in the right posterior cingulate gyrus and the bilateral primary visual cortices. Decreased alpha activity (i.e., more negative) during the retrieval phase were observed in the lateral occipital cortices, left supramarginal gyrus (SMG), and left angular gyrus. Similarly, decreased beta oscillations (i.e., more negative) during the retrieval phase were found in the lateral occipital cortices, bilateral primary motor cortices, and bilateral superior parietal cortices.

To statistically examine the effects of healthy aging on the neural dynamics serving WM function, we subjected the frequency-specific whole-brain encoding, maintenance, and retrieval participant-level average maps to correlation analysis. These whole-brain correlation analyses were then followed by cluster-based permutation testing to correct for multiple comparisons. These analyses revealed that theta oscillations during encoding became significantly stronger as a function of age in the left primary visual cortex (p = .037, corrected) and left dlPFC (p = .045, corrected; Figure 14), and that there were no age-related theta effects during the maintenance or retrieval phases. In contrast, the decreases in alpha and beta became stronger (i.e., more negative) with increasing age throughout all phases of WM processing (i.e., encoding, maintenance, and retrieval; Figure 15). During the encoding phase, decreases in alpha

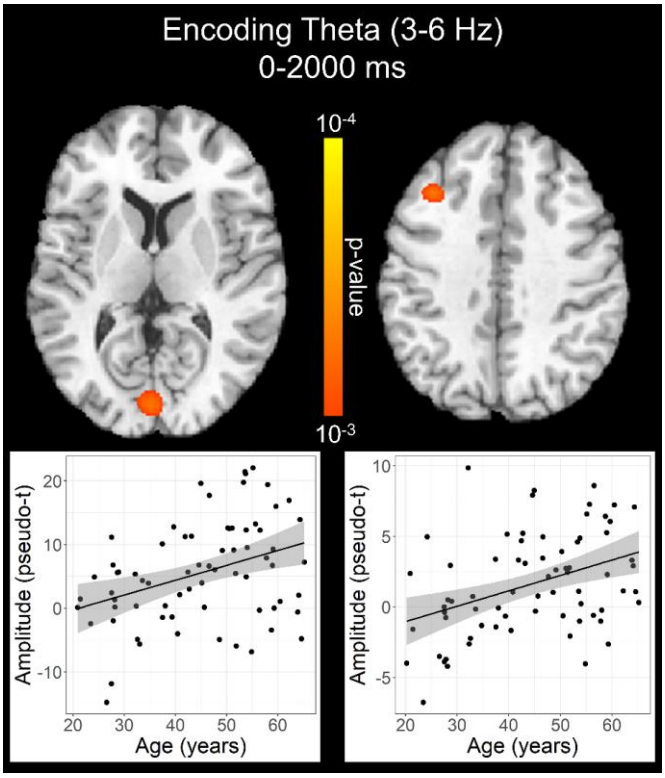

Figure 14. Effect of age on theta oscillations during the encoding phase.

Whole-brain linear regression analysis revealed that theta activity increased in the left primary visual cortex and left dlPFC with older age. Linear regression plots of peak voxel pseudo-t values are shown as a function of age. Lines of best-fit and 95% CI (shaded area) are overlaid.

became stronger (i.e., more negative) as a function of age in the left middle frontal gyrus (p = .023, corrected) and the left anterior cingulate gyrus (p = .033, corrected). This age-related change in activity in the left middle frontal gyrus was sustained through the maintenance phase (p = .029, corrected), along with stronger decreases in alpha/band responses (i.e., more negative) in the left dlPFC (p = .031, corrected). During the retrieval phase, decreases in alpha oscillations also became stronger (i.e., more negative) as a function of age in the left insula (p = .009, corrected), left anterior cingulate (p = .020, corrected), and left middle temporal gyrus (p = .031, corrected). Finally, the decreases in beta oscillations (14-19 Hz) during the retrieval phase were found to get stronger (i.e., more negative) with increasing age in the left primary motor

cortex (p < .001, corrected), right primary somatosensory cortex (p < .001, corrected), bilateral superior parietal cortices (ps < .001, corrected), left dlPFC (p = .007, corrected), and left anterior superior temporal gyrus (p = .020, corrected). A complete summary of all significant effects can be found in Table 2.

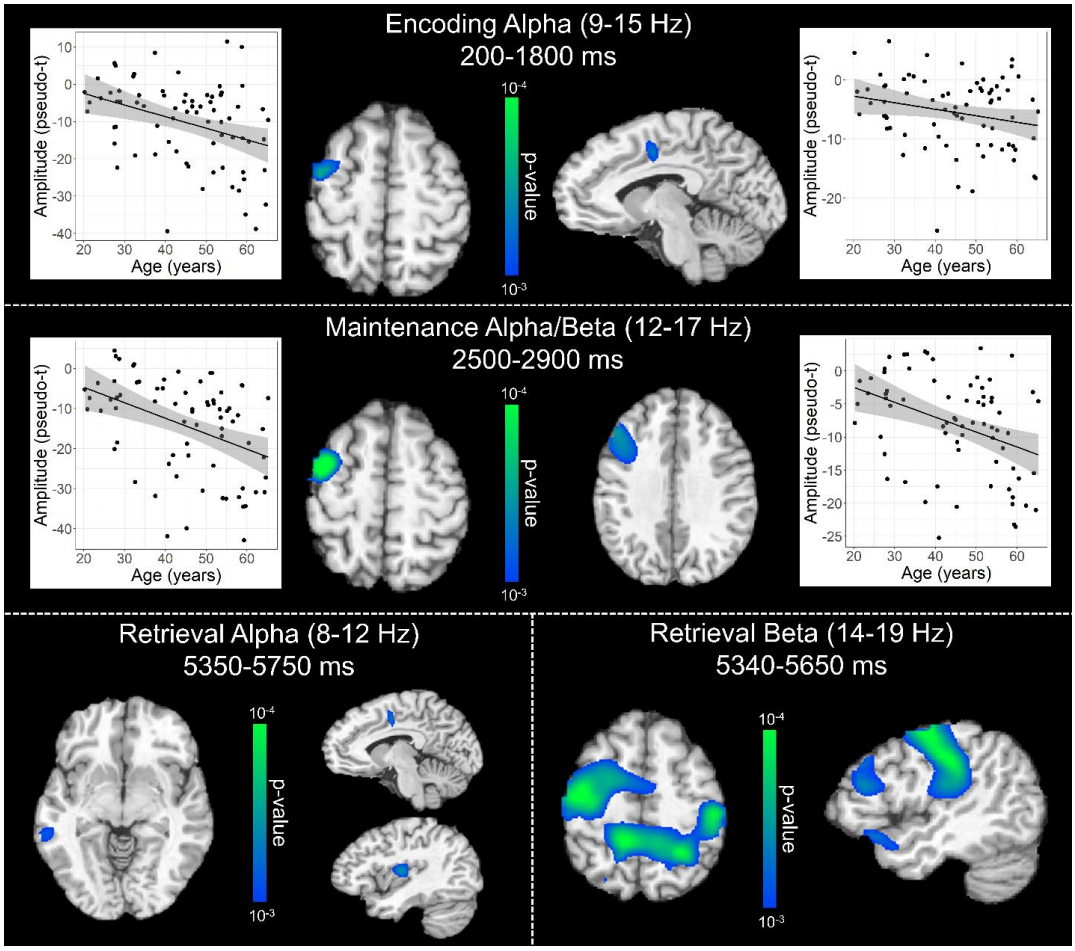

Figure 15. Effect of age on alpha and beta oscillations during the encoding, maintenance, and retrieval phases.

Whole-brain linear regression analyses testing for age-related changes in alpha (encoding and retrieval), alpha/beta (maintenance), and beta (retrieval) are shown during the encoding (top), maintenance (middle), and retrieval bottom) phases. During encoding (top), decreases in alpha activity became significantly stronger (i.e., more negative relative to baseline), as a function of age, in prefrontal cortical regions and anterior cingulate. Additionally, age-related alterations in alpha and beta activity during the maintenance period (middle) were found in the left prefrontal cortices, while age-related effects during retrieval (bottom) were observed across a diverse set of brain regions that have been implicated in working memory processing (i.e., frontal, temporal, and parietal cortices). Beyond statistical maps, linear regression plots of peak voxel pseudo-t values are shown as a function of age for encoding and maintenance peaks. Lines of best-fit and 95% CI (shaded area) are overlaid.

Region/Effect of Interest	Frequency	X	Y	Z	*df*	Statistic
Encoding						***r***
Left primary visual cortex	θ	-2	-85	10	70	.42
Left dlPFC	θ	-34	24	38	70	.40
Left middle frontal gyrus	α	-42	-5	54	74	-.41
Left anterior cingulate gyrus	α	-10	-5	42	74	-.40
Maintenance						***r***
Left middle frontal gyrus	α/β	-42	-1	54	72	-.42
Left dlPFC	α/β	-42	28	42	72	-.42
Retrieval						***r***
Left insula	α	-30	-13	10	72	-.41
Left anterior cingulate gyrus	α	-6	-5	42	72	-.40
Left middle temporal gyrus	α	-58	-37	-3	72	-.39
Left primary motor cortex	β	-42	-13	50	71	-.45
Right primary somatosensory cortex	β	42	-21	42	71	-.46
Left superior parietal cortex	β	-14	-45	54	71	-.45
Right superior parietal cortex	β	30	-53	58	71	-.45
Left dlPFC	β	-50	32	22	71	-.41
Left anterior superior temporal gyrus	β	-50	24	-11	71	-.41

Table 2. Coordinates of the peak response in each significant age correlation cluster.

All test statistics are significant at $p < .001$ level and survive cluster-based permutation testing. All coordinates are in Talairach space. dlPFC = dorsolateral prefrontal cortex. *df* = degrees of freedom.

Finally, we investigated the relationship between cognitive performance and neural oscillatory activity. We found a significant negative relationship between executive function and alpha/beta oscillatory activity during all phases of working memory, such that stronger decreases in alpha/beta amplitude predicted better executive function scores (Figure 16). Specifically, significant negative relationships were found between executive functioning and alpha activity in the left middle frontal gyrus (r_{68} = -.241, p = .045) during the encoding period, alpha/beta activity in the middle frontal gyrus (r_{67} = -.384, p = .001) and in the dlPFC (r_{68} = -.285, p = .017) during the maintenance period, and beta activity in the dlPFC (r_{68} = -.261, p = .029) during the retrieval period.

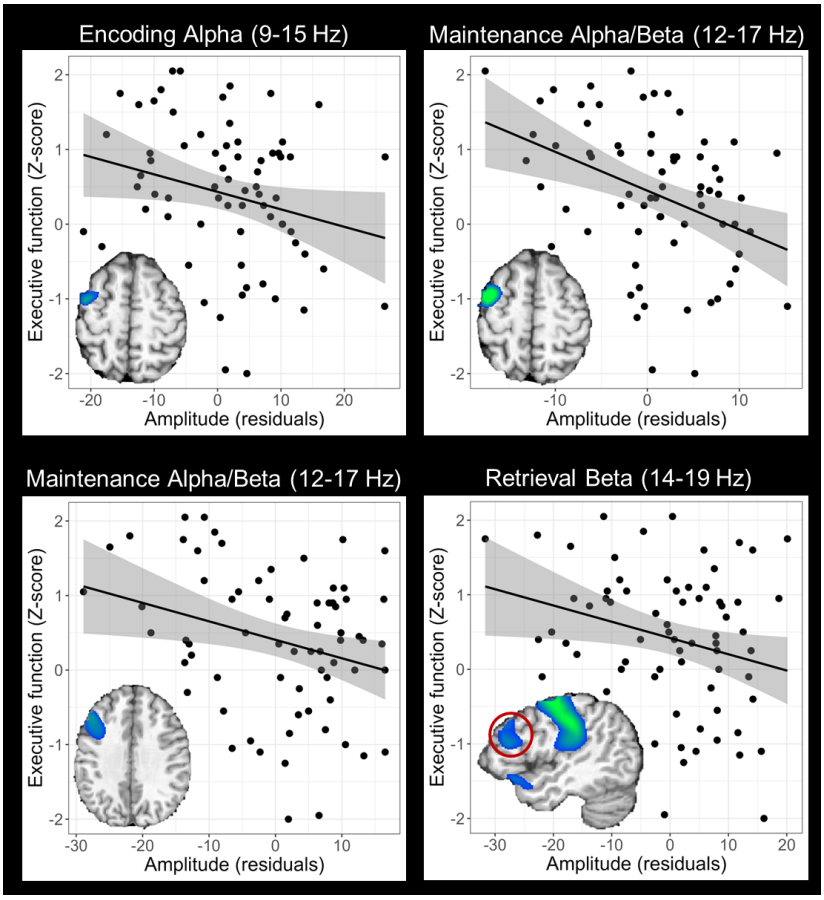

Figure 16. Relationship between executive function outside the scanner and alpha/beta activity during encoding, maintenance, and retrieval phases.

Across all participants, the strength of the alpha/beta decreases in activity were negatively correlated with executive function. Such that stronger decreases in alpha/beta activity predicted better executive functioning. Line of best linear fit and 95% CI (i.e., shaded area) are shown.

Discussion:

In the present study, we investigated the effect of healthy aging on the neural oscillatory dynamics serving verbal WM processing using MEG and advanced source reconstruction. Similar to previous studies utilizing a modified Sternberg WM task in healthy aging adults, we found that reaction time increased with age and that there were no significant aging effects on task accuracy (35, 234). Across all participants, our results also showed that WM processing is supported by regionally distinct neural oscillations in the theta, alpha, and beta bands throughout all phases (i.e., encoding, maintenance, and retrieval) and that such activity is broadly affected by healthy aging.

Briefly, theta oscillations were shown to become stronger in the primary visual cortices and in the frontal cortex with increasing age. Furthermore, throughout all WM phases and in several frontal, parietal, and temporal regions, alpha, beta, and alpha/beta activity became stronger (i.e., more negative) as a function of age. Importantly, across all participants, stronger decreases in alpha/beta activity in these prefrontal regions predicted better executive functioning, supporting the compensatory nature of these responses. Critically, these results represent the first oscillatory analysis of verbal WM function in a healthy aging sample in which neural activity was examined throughout all phases of processing, including the retrieval stage. Below, we discuss the implications of these novel findings on our understanding of how healthy aging affects verbal WM processing.

Across all frequencies, our findings demonstrate widespread and robust cortical activation patterns during verbal working memory task performance, as well as age-related changes in these neural activations. These task-related activations and age-related changes are most prevalent in the occipital, parietal, and frontal cortices; regions which have been shown to be critical to verbal working memory performance (202, 203). According to the theories of working memory function originally proposed by Baddeley and colleagues, the neural subsystems serving working memory processing include the visuospatial sketchpad, phonological loop, episodic buffer, and the central executive (235, 236). The visuospatial sketchpad is responsible for processing the visual and spatial components of a stimulus, and is served by the occipital and parieto-temporal cortices (202, 203). The phonological loop deals with the processing and rehearsal of auditory and language information. Further, the phonological loop is a predominately left hemispheric network comprised of the phonological store in the parietal lobe (202, 237), which briefly stores fleeting memory traces, and the articulatory process in the inferior frontal gyrus and superior temporal gyrus (e.g., Broca's area; 238, 239, 240),

responsible for the rehearsal and manipulation of information in the phonological store (e.g., through subvocal repetition). The episodic buffer is a more distributed subsystem which links working memory and long-term memory, facilitating the integration of information from separate modalities (i.e., visual, spatial, auditory, language, etc.) and binding information into coherent episodes (236). Finally, the central executive component exerts top-down control over the other working memory subsystems, via the allocation of attentional resources and direction of information flow to the other subsystems, and is thought be housed in the prefrontal cortex (203, 204). Considering the letter-based stimuli utilized in our modified Sternberg working memory task, we expected robust activation of each of the aforementioned subsystems.

One of our most interesting findings was the broad strengthening of alpha and beta oscillations (i.e., decreases from baseline) with increasing age. The local suppression of alpha and beta activity, relative to baseline levels, has been shown to represent active cortical engagement (i.e., active visual processing in higher-order visual areas) (35, 171-173, 241). This is further supported by multimodal studies which have demonstrated co-localization of decreases in alpha and beta activity with increased BOLD fMRI signal during cognitive tasks (242, 243). During the encoding phase, older individuals showed significantly stronger decreases in alpha activity (i.e., more negative relative to baseline) in the left middle frontal gyrus (MFG) and the left anterior cingulate. This significant age-related shift in left MFG activity extended into the maintenance period, with the addition of age-related effects in alpha/beta activity in the left dlPFC. These prefrontal cortical regions are thought to act as central executive nodes during WM task performance, allowing for the allocation of WM subsystem resources and the direction of attention (203, 204). These findings of age-related increases in frontal regions are in widespread agreement with the aging literature, which has demonstrated that increased prefrontal neural recruitment can offset declines in cognitive performance

as a function of healthy aging (i.e., CRUNCH: 20, 212, 215, 218, 221-223). Further supporting this compensation hypothesis, we found that, across all participants, stronger decreases in alpha/beta activity predicted better executive functioning. Of note, we found no significant age-related changes during the encoding and maintenance phases in alpha/beta activity in either visual processing or language areas, which have historically been linked to the visuospatial sketchpad and phonological loop, respectively (202, 203, 237). In sum, the present work is in agreement with our hypotheses that older adults would require stronger engagement of left hemispheric frontal WM hubs and reinforces previous aging WM literature in demonstrating how crucial increased neural activity in prefrontal cortices is for older individuals during WM processing.

Beyond the encoding and maintenance phases, we found significant alpha and beta oscillatory changes as a function of age during the retrieval phase. Though previous studies have extensively characterized neural activity during WM encoding and maintenance, studies analyzing the neural dynamics during the retrieval phase are sparse. During the retrieval phase, older participants showed stronger decreases in alpha activity (i.e., more negative) in the left posterior middle temporal gyrus (MTG), left insula, and left anterior cingulate. Additionally, beta activity during the retrieval phase decreased (i.e., more negative) with increasing age in the left primary motor cortex, bilateral superior parietal cortices, left dlPFC, left anterior superior temporal gyrus, and other regions. Thus, unlike the age-related alpha/beta effects observed during the encoding and maintenance phases, which were largely confined to prefrontal cortices, age-related changes in alpha/beta activity during the retrieval phase were found to extend to other WM subsystems. Specifically, in the retrieval phase, older individuals tended to more strongly engage neural regions linked to higher-order visual processing (i.e., visuospatial sketchpad; left posterior MTG), language processing (i.e., left STG), phonological storage (i.e., superior parietal lobes), central executive processes (i.e., left

dlPFC), and motor execution (i.e., primary motor cortex). These retrieval phase findings are in line with our hypothesis that older adults would more strongly recruit left hemispheric frontal and parieto-occipital WM nodes, relative to younger participants. As noted above, only a few studies have examined the retrieval stage, Guran and associates (244) found that older (i.e., 53-80 years) compared to younger (i.e., 18-30 years) individuals had stronger alpha/beta decreases relative to baseline in sensors overlying frontal, central, and parietal regions (244), which is consistent with our findings. Finally, our finding of stronger decreases in beta (i.e., more negative) in the primary motor cortex in older participants is consistent with work from the motor control literature (122, 123). Thus, this effect of aging on motor beta activity is likely task independent.

We also found robust age-related effects in the theta range. Theta oscillations in the primary visual cortex have been widely implicated in basic visual processing, while frontal theta activity has been shown to be important for the higher-order organization and maintenance of stimulus information (201, 205-207, 241, 245). Though theta activity has been shown to be critical for WM function, age-related changes in these theta band dynamics have only been weakly characterized. Age-related theta alterations in the current study were found to be confined to the encoding phase, with activity in the primary visual cortex and left dlPFC getting stronger as a function of increasing age. One comparable study found that older participants (i.e., 62-71 years) were more susceptible to WM disruption and that frontal midline theta was stronger in older individuals (i.e., 19-29 years; 246). Our findings of age-related increases in theta activity, particularly those in the dlPFC, are consistent with our alpha and beta band findings and the neural compensation hypothesis (i.e., CRUNCH). Additionally, theta band activity in the PFC of healthy young adults during WM performance has been shown to increase stepwise with increasing task load (205, 207, 241), further supporting the idea that the increased theta activity with increasing age may represent these older individuals

needing to exert more neural resources to complete this WM task (i.e., less efficient processing). Altogether, in conjunction with our alpha and beta findings, we have demonstrated that the widely cited age-related increases in neural recruitment are not frequency specific, with age-related effects spanning multiple frequency bands (i.e., theta, alpha, and beta) and working memory subsystems.

Interestingly, our results did not show the hypothesized and commonly reported age-related change in the lateralization of prefrontal activation. Specifically, previous work has demonstrated that younger individuals more strongly utilize left hemispheric prefrontal regions during working memory performance, compared to older individuals who exhibit more bilateral prefrontal activity (15, 16, 35, 215, 220, 221). This discrepancy may be due to study design and analysis differences. Firstly, our sample of 78 health adults is nearly double the size of most previous healthy aging WM studies and our whole-brain data were modeled using age as a continuous variable, compared to dichotomizing age groups as has commonly been done (16, 35, 215, 221). Secondly, the current study utilized cluster-based permutation testing of the source images to strongly control for false positives, compared to the much less stringent multiple comparison correction approaches that have previously been used (e.g., uncorrected or cluster-size corrections) (16, 35, 221). Finally, the oldest participants in the current study were younger (i.e., 65 years) than many aging WM studies (e.g., 75-82 years) (15, 16, 215, 221). Thus, our relatively younger participants may not have reached a level of cognitive dysfunction that necessitates bilateral prefrontal recruitment, but future studies are needed to confirm these findings.

Before closing, it is important to note the limitations of this study. First, as mentioned above, the oldest participants in our sample were slightly younger (i.e., 65 years) than some previous WM studies of aging (e.g., 75-82 years). For future studies, increasing the age of the oldest participants would allow for the hypothesized transition

from age-related compensation (i.e., increased neural activity and normal accuracy) to age-related decompensation (i.e., decreased neural activity and decreased accuracy) to be more thoroughly studied. Finally, the modified Sternberg WM paradigm that was utilized for the current study required that participants remember six letter stimuli per trial and previous work has shown that varying the cognitive load of WM tasks leads to an interesting pattern of effects in older individuals (i.e., greater neural activity at low working memory loads with decompensation and decreased neural activity at higher working memory loads) (212, 215, 218-220). Thus, future aging WM research would benefit from having multiple memory load conditions of varying difficulty.

Taken together, these data support the previous literature showing greater recruitment of the prefrontal cortex in older individuals during WM performance to maintain similar performance to younger individuals. Importantly, our findings extend this literature by demonstrating that age-related hyperactivation of prefrontal regions occurs in all phases of WM (i.e., encoding, maintenance, and retrieval) and is multispectral involving theta, alpha, and beta oscillatory activity. Further, though the age-related changes in alpha and beta band activity were restricted to prefrontal executive control regions during the encoding and maintenance phases, these age-related changes emerged in a more widespread network that included language (i.e., phonological loop) and motor regions during the retrieval phase. Developing a better understanding of these age-related alterations in WM function may have important implications for developing targeted interventions aimed at improving cognitive function and promoting healthy aging across the lifespan.

CONCLUSIONS

These studies demonstrate that healthy aging is associated with neural oscillatory changes in both lower- and higher-order cognitive functions. Importantly, the direction of these age-related neural changes were not only domain specific, but also frequency-dependent with differential alterations to theta, alpha, beta, and gamma oscillatory activity. While broadly aligning with previous healthy aging electrophysiologic and non-electrophysiologic (i.e., fMRI and PET) research, our findings extended this literature by performing analyses in a frequency- and time-resolved manner and by identifying the cortical origins of each age-related change. Taken together, these studies provide potential targets for therapeutic intervention and provide critical normative aging data for comparison with pathological aging (e.g., Alzheimer's disease).

With regard to visual entrainment, we found that healthy aging was associated with decreased overall entrainment amplitude, as well as increased latency of these entrainment responses. Additionally, differential changes in occipital gamma band oscillations to visual gratings stimuli were observed as a function of age. Specifically, we found an age-related increase in the gamma onset response and a decrease in the gamma offset response. Further, the decline in gamma offset response amplitude predicted reduced processing speed. Importantly, in each of these studies (Chapters 1 and 2), no age-related alterations in visual theta, alpha, or beta oscillations were observed. Together, these studies demonstrate that age-related changes in visual cortical responses are not ubiquitous, but are instead dependent on stimulation type (e.g., entrainment) and response frequency (i.e., theta, alpha, beta, and gamma).

Most previous electrophysiologic research investigating basic visual processing in healthy aging did so using sensor- or electrode-level event-related potential (ERP) or event-related field analyses (66-73). These analyses typically involve trial-wise

averaging and frequency filtering of the data, which results in a loss of induced signals (i.e., non-phase locked), loss of frequency specificity (due to collapsing across lower frequencies; ~1-30 Hz), and loss of higher frequency activity (i.e., >30 Hz). Our findings of age-related decreases in entrainment response amplitude and increased latency (Chapter 1) are in agreement with previous ERP studies, however, our visual gamma oscillatory results (Chapter 2) are not comparable to these previous analyses due to the aforementioned bandpass filtering utilized in these analyses. However, previous human and animal studies have demonstrated a strong association between gamma band oscillations and the fMRI blood-oxygen-level-dependent (BOLD) signal (242, 247). To date, fMRI-based analyses of visual processing in healthy aging have yielded mixed results, with some researchers finding age-related decreases in visual cortical activity (75-78) while others found no significant change (79-81). Considering our findings of differential aging effects on the gamma visual response (i.e., stronger onset and weaker offset), these conflicting fMRI results are not especially surprising considering the poor temporal resolution of the BOLD fMRI signal, which effectively smears together the distinct age-related changes in each phase of visual processing (i.e., onset, sustained, and offset). Together, these data demonstrate how critical it is that future research into age-related alterations in visual processing utilizes neuroimaging modalities with high temporal resolution (e.g., EEG and MEG) and data processing pipelines which maintain separation of distinct oscillatory frequencies.

During verbal working memory (VWM) performance, we found that older individuals had stronger theta, alpha, and beta band responses throughout all working memory phases (i.e., encoding, maintenance, and retrieval). These age-related changes in neural activity were largely in the prefrontal and parietal areas, which is in agreement with the CRUNCH model. Further, in conjunction with our entrainment results (Chapter 1), our findings support the PASA hypothesis of healthy aging, with older individuals

showing weaker posterior cortical activity (i.e., decreased entrainment amplitudes) along with stronger anterior cortical activity (i.e., increased WM prefrontal activity). However, our analyses of higher frequency visual oscillations (i.e., gamma; Chapter 2) demonstrate that not all visual responses display a clear decrease in amplitude as a function of age.

Under the CRUNCH hypothesis, individuals are expected to recruit greater neural resources to accommodate increased cognitive demands (e.g., increased task difficulty, age-related neural inefficiency, etc.). Thus, increased neural activity is expected to predict better cognitive performance. Conversely, once cognitive demand exceeds neural reserves, neural activity is expected to decrease along with cognitive performance. Further, the PASA model posits that the purpose of the increased prefrontal activity is to counteract the age-related posterior sensory deficits. Our visual gamma (Chapter 2) and VWM (Chapter 3) results both align with these expectations. Specifically, activity in several fronto-parietal areas, which displayed *age-related strengthening* of alpha/beta decreases in activity, was shown to predict *better* executive function scores across all participants. Further, decreases in primary visual cortical gamma offset response amplitude, which displayed *age-related weakening*, were shown to predict *worse* processing speed domain scores across all participants. Together, these brain-behavior relationships support previous neurocognitive theories of aging and extend this literature by demonstrating that these age-related effects are frequency-specific (i.e., gamma in Chapter 2 and alpha/beta in Chapter 3). Of note, future studies would greatly benefit from experimentally manipulating task difficulty as a variable of interest. Not only does task difficulty heavily influence age-related neural responses, but neglecting to control and manipulate task difficulty makes comparing results across studies much more difficult.

In conclusion, our studies demonstrate cognitive domain-specific patterns of neural oscillatory changes which occur during healthy aging. Broadly, our results were in agreement with previous neural aging research, however, the spectral specificity of our findings draw attention to the lack of previous healthy aging research which has used time- and frequency-resolved approaches. Such analyses will prove crucial for developing a more complete understanding of how healthy aging affects neural processes. Another important area for future research is accessing how these age-related changes in neural oscillatory responses can be targeted for noninvasive neuromodulation (e.g., cognitive training, pharmacological treatment, non-invasive stimulation). Specifically, with the use of non-invasive brain stimulation methods such as transcranial magnetic stimulation (TMS), direct current stimulation (tDCS), and alternating current stimulation (tACS), these regionally-specific age-related neural changes may serve as targets for researchers to facilitate age-related neural compensatory processes and ameliorate pathological changes. Finally, the study of neural changes during healthy aging not only expands our knowledge of these “normal” neurologic alterations, but also provides much needed normative groundwork for comparison against populations with age-related neurocognitive disorders (e.g., Alzheimer’s disease, Parkinson’s disease, Dementia with Lewy Bodies).

BIBLIOGRAPHY

1. Ageing and Health: World Health Organization (WHO); 2022 [Available from: https://www.who.int/news-room/fact-sheets/detail/ageing-and-health.

2. Hedden T, Gabrieli JDE. Insights into the ageing mind: a view from cognitive neuroscience. Nature Reviews Neuroscience. 2004;5(2):87-96.

3. Murman DL. The Impact of Age on Cognition. Semin Hear. 2015;36(3):111-21.

4. Tucker-Drob EM, de la Fuente J, Köhncke Y, Brandmaier AM, Nyberg L, Lindenberger U. A strong dependency between changes in fluid and crystallized abilities in human cognitive aging. Sci Adv. 2022;8(5):eabj2422.

5. Cattell RB. Theory of fluid and crystallized intelligence: A critical experiment. Journal of Educational Psychology. 1963;54(1):1-22.

6. Salthouse TA. When does age-related cognitive decline begin? Neurobiology of Aging. 2009;30(4):507-14.

7. Resnick SM, Pham DL, Kraut MA, Zonderman AB, Davatzikos C. Longitudinal Magnetic Resonance Imaging Studies of Older Adults: A Shrinking Brain. The Journal of Neuroscience. 2003;23(8):3295-301.

8. Dickstein DL, Kabaso D, Rocher AB, Luebke JI, Wearne SL, Hof PR. Changes in the structural complexity of the aged brain. Aging Cell. 2007;6(3):275-84.

9. Pannese E. Morphological changes in nerve cells during normal aging. Brain Structure and Function. 2011;216(2):85-9.

10. Gunning-Dixon FM, Raz N. The cognitive correlates of white matter abnormalities in normal aging: a quantitative review. Neuropsychology. 2000;14(2):224-32.

11. Raz N, Gunning-Dixon F, Head D, Rodrigue KM, Williamson A, Acker JD. Aging, sexual dimorphism, and hemispheric asymmetry of the cerebral cortex: replicability of regional differences in volume. Neurobiol Aging. 2004;25(3):377-96.

12. DeCarli C, Massaro J, Harvey D, Hald J, Tullberg M, Au R, et al. Measures of brain morphology and infarction in the framingham heart study: establishing what is normal. Neurobiol Aging. 2005;26(4):491-510.

13. Festini SB, Zahodne LB, Reuter-Lorenz PA. Theoretical Perspectives on Age Differences in Brain Activation: HAROLD, PASA, CRUNCH—How Do They STAC Up? Oxford Research Encyclopedia of Psychology. 2018.

14. Cabeza R. Hemispheric asymmetry reduction in older adults: the HAROLD model. Psychol Aging. 2002;17(1):85-100.

15. Cabeza R, Daselaar SM, Dolcos F, Prince SE, Budde M, Nyberg L. Task-independent and task-specific age effects on brain activity during working memory, visual attention and episodic retrieval. Cereb Cortex. 2004;14(4):364-75.

16. Reuter-Lorenz PA, Jonides J, Smith EE, Hartley A, Miller A, Marshuetz C, et al. Age Differences in the Frontal Lateralization of Verbal and Spatial Working Memory Revealed by PET. Journal of Cognitive Neuroscience. 2000;12(1):174-87.

17. Maillet D, Rajah MN. Age-related differences in brain activity in the subsequent memory paradigm: a meta-analysis. Neurosci Biobehav Rev. 2014;45:246-57.

18. Li H-J, Hou X-H, Liu H-H, Yue C-L, Lu G-M, Zuo X-N. Putting age-related task activation into large-scale brain networks: A meta-analysis of 114 fMRI studies on healthy aging. Neuroscience & Biobehavioral Reviews. 2015;57:156-74.

19. Davis SW, Dennis NA, Daselaar SM, Fleck MS, Cabeza R. Que PASA? The Posterior-Anterior Shift in Aging. Cerebral Cortex. 2008;18(5):1201-9.

20. Reuter-Lorenz PA, Cappell KA. Neurocognitive aging and the compensation hypothesis. Current Directions in Psychological Science. 2008;17:177-82.

21. Dennis NA, Cabeza R. Neuroimaging of healthy cognitive aging. The handbook of aging and cognition, 3rd ed. New York, NY, US: Psychology Press; 2008. p. 1-54.

22. Rossi S, Miniussi C, Pasqualetti P, Babiloni C, Rossini PM, Cappa SF. Age-Related Functional Changes of Prefrontal Cortex in Long-Term Memory: A Repetitive Transcranial Magnetic Stimulation Study. The Journal of Neuroscience. 2004;24(36):7939-44.

23. Solé-Padullés C, Bartrés-Faz D, Junqué C, Clemente IC, Molinuevo JL, Bargalló N, et al. Repetitive Transcranial Magnetic Stimulation Effects on Brain Function and Cognition among Elders with Memory Dysfunction. A Randomized Sham-Controlled Study. Cerebral Cortex. 2006;16(10):1487-93.

24. Buzsaki G, Draguhn A. Neuronal oscillations in cortical networks. Science. 2004;304(5679):1926-9.

25. Rempe MP, Ott LR, Picci G, Penhale SH, Christopher-Hayes NJ, Lew BJ, et al. Spontaneous cortical dynamics from the first years to the golden years. Proceedings of the National Academy of Sciences. 2023;120(4).

26. Uhlhaas PJ, Singer W. Abnormal neural oscillations and synchrony in schizophrenia. Nature Reviews Neuroscience. 2010;11(2):100-13.

27. Simon DM, Wallace MT. Dysfunction of sensory oscillations in Autism Spectrum Disorder. Neuroscience & Biobehavioral Reviews. 2016;68:848-61.

28. Foffani G, Alegre M. Brain oscillations and Parkinson disease. Handb Clin Neurol. 2022;184:259-71.

29. Casagrande CC, Rempe MP, Springer SD, Wilson TW. Comprehensive review of task-based neuroimaging studies of cognitive deficits in Alzheimer's disease using electrophysiological methods. Ageing Res Rev. 2023;88:101950.

30. Stier C, Braun C, Focke NK. Adult lifespan trajectories of neuromagnetic signals and interrelations with cortical thickness. Neuroimage. 2023;278:120275.

31. Finley AJ, Angus DJ, Knight E, Van Reekum CM, Lachman ME, Davidson RJ, et al. Resting EEG Periodic and Aperiodic Components Predict Cognitive Decline Over 10 Years. 2023.

32. Tröndle M, Popov T, Pedroni A, Pfeiffer C, Barańczuk-Turska Z, Langer N. Decomposing age effects in EEG alpha power. Cortex. 2023;161:116-44.

33. Karlsson AE, Wehrspaun CC, Sander MC. Item recognition and lure discrimination in younger and older adults are supported by alpha/beta desynchronization. Neuropsychologia. 2020;148:107658.

34. Arif Y, Spooner RK, Wiesman AI, Embury CM, Proskovec AL, Wilson TW. Modulation of attention networks serving reorientation in healthy aging. Aging. 2020;12(13):12582-97.

35. Proskovec AL, Heinrichs-Graham E, Wilson TW. Aging modulates the oscillatory dynamics underlying successful working memory encoding and maintenance. Human Brain Mapping. 2016;37(6):2348-61.

36. Gajewski PD, Falkenstein M. Age-Related Effects on ERP and Oscillatory EEG-Dynamics in a 2-Back Task. Journal of Psychophysiology. 2014;28:162-77.

37. Barr MS, Radhu N, Guglietti CL, Zomorrodi R, Rajji TK, Ritvo P, et al. Age-related differences in working memory evoked gamma oscillations. Brain Res. 2014;1576:43-51.

38. Gola M, Magnuski M, Szumska I, Wróbel A. EEG beta band activity is related to attention and attentional deficits in the visual performance of elderly subjects. International Journal of Psychophysiology. 2013;89(3):334-41.

39. Küçük KM, Wienke AS, Mathes B, Başar-Eroğlu C. Multistable perception elicits compensatory alpha activity in older adults. Front Aging Neurosci. 2023;15:1136124.

40. Laera G, Arcara G, Gajewski PD, Kliegel M, Hering A. Age-related modulation of EEG time-frequency responses in prospective memory retrieval. Neuropsychologia. 2021;155:107818.

41. Murty D, Manikandan K, Kumar WS, Ramesh RG, Purokayastha S, Javali M, et al. Gamma oscillations weaken with age in healthy elderly in human EEG. Neuroimage. 2020;215:116826.

42. Elshafei HA, Fornoni L, Masson R, Bertrand O, Bidet-Caulet A. Age-related modulations of alpha and gamma brain activities underlying anticipation and distraction. PLOS ONE. 2020;15(3):e0229334.

43. Alperin BR, Mott KK, Rentz DM, Holcomb PJ, Daffner KR. Investigating the age-related “anterior shift” in the scalp distribution of the <scp>P3b</scp> component using principal component analysis. Psychophysiology. 2014;51(7):620-33.

44. Deiber M-P, Ibañez V, Missonnier P, Rodriguez C, Giannakopoulos P. Age-associated modulations of cerebral oscillatory patterns related to attention control. NeuroImage. 2013;82:531-46.

45. Vaden RJ, Hutcheson NL, McCollum LA, Kentros J, Visscher KM. Older adults, unlike younger adults, do not modulate alpha power to suppress irrelevant information. NeuroImage. 2012;63(3):1127-33.

46. Elliott DB, Yang KC, Whitaker D. Visual acuity changes throughout adulthood in normal, healthy eyes: seeing beyond 6/6. Optom Vis Sci. 1995;72(3):186-91.

47. Trick GL, Silverman SE. Visual sensitivity to motion: age-related changes and deficits in senile dementia of the Alzheimer type. Neurology. 1991;41(9):1437-40.

48. Burton KB, Owsley C, Sloane ME. Aging and neural spatial contrast sensitivity: photopic vision. Vision Res. 1993;33(7):939-46.

49. Elliott D, Whitaker D, MacVeigh D. Neural contribution to spatiotemporal contrast sensitivity decline in healthy ageing eyes. Vision Res. 1990;30(4):541-7.

50. Erdinest N, London N, Lavy I, Morad Y, Levinger N. Vision through Healthy Aging Eyes. Vision (Basel). 2021;5(4).

51. Brenner MH, Curbow B, Javitt JC, Legro MW, Sommer A. Vision change and quality of life in the elderly. Response to cataract surgery and treatment of other chronic ocular conditions. Arch Ophthalmol. 1993;111(5):680-5.

52. Owsley C, Ball K, McGwin G, Jr., Sloane ME, Roenker DL, White MF, et al. Visual processing impairment and risk of motor vehicle crash among older adults. JAMA. 1998;279(14):1083-8.

53. Sakai H, Uchiyama Y, Takahara M, Doi S, Kubota F, Yoshimura T, et al. Is the useful field of view a good predictor of at-fault crash risk in elderly Japanese drivers? Geriatr Gerontol Int. 2015;15(5):659-65.

54. Lord SR, Dayhew J, Howland A. Multifocal glasses impair edge-contrast sensitivity and depth perception and increase the risk of falls in older people. J Am Geriatr Soc. 2002;50(11):1760-6.

55. Frangou S, Modabbernia A, Williams SCR, Papachristou E, Doucet GE, Agartz I, et al. Cortical thickness across the lifespan: Data from 17,075 healthy individuals aged 3-90 years. Hum Brain Mapp. 2021;43(1):431-51.

56. Fjell AM, Westlye LT, Amlien I, Espeseth T, Reinvang I, Raz N, et al. High consistency of regional cortical thinning in aging across multiple samples. Cereb Cortex. 2009;19(9):2001-12.

57. Allen JS, Bruss J, Brown CK, Damasio H. Normal neuroanatomical variation due to age: the major lobes and a parcellation of the temporal region. Neurobiol Aging. 2005;26(9):1245-60; discussion 79-82.

58. Griffis JC, Burge WK, Visscher KM. Age-Dependent Cortical Thinning of Peripheral Visual Field Representations in Primary Visual Cortex. Front Aging Neurosci. 2016;8:248.

59. Salat DH, Buckner RL, Snyder AZ, Greve DN, Desikan RS, Busa E, et al. Thinning of the cerebral cortex in aging. Cereb Cortex. 2004;14(7):721-30.

60. Thambisetty M, Wan J, Carass A, An Y, Prince JL, Resnick SM. Longitudinal changes in cortical thickness associated with normal aging. NeuroImage. 2010;52(4):1215-23.

61. Hirano Y, Oribe N, Onitsuka T, Kanba S, Nestor PG, Hosokawa T, et al. Auditory Cortex Volume and Gamma Oscillation Abnormalities in Schizophrenia. Clin EEG Neurosci. 2020;51(4):244-51.

62. Moretti DV, Paternicò D, Binetti G, Zanetti O, Frisoni GB. EEG upper/low alpha frequency power ratio relates to temporo-parietal brain atrophy and memory performances in mild cognitive impairment. Front Aging Neurosci. 2013;5:63.

63. Muthukumaraswamy SD, Singh KD, Swettenham JB, Jones DK. Visual gamma oscillations and evoked responses: variability, repeatability and structural MRI correlates. Neuroimage. 2010;49(4):3349-57.

64. Palaniyappan L, Doege K, Mallikarjun P, Liddle E, Francis-Liddle P. Cortical thickness and oscillatory phase resetting: a proposed mechanism of salience network dysfunction in schizophrenia. Psychiatriki. 2012;23(2):117-29.

65. van Pelt S, Shumskaya E, Fries P. Cortical volume and sex influence visual gamma. Neuroimage. 2018;178:702-12.

66. Armstrong RA, Slaven A, Harding GF. The influence of age on the pattern and flash visual evoked magnetic response (VEMR). Ophthalmic Physiol Opt. 1991;11(1):71-5.

67. Polich J. EEG and ERP assessment of normal aging. Electroencephalography and Clinical Neurophysiology/Evoked Potentials Section. 1997;104(3):244-56.

68. Kavcic V, Martin T, Zalar B. Aging effects on visual evoked potentials (VEPs) for motion direction discrimination. Int J Psychophysiol. 2013;89(1):78-87.

69. Störmer VS, Li S-C, Heekeren HR, Lindenberger U. Normal Aging Delays and Compromises Early Multifocal Visual Attention during Object Tracking. Journal of Cognitive Neuroscience. 2013;25(2):188-202.

70. Celesia GG, Daly RF. Effects of aging on visual evoked responses. Arch Neurol. 1977;34(7):403-7.

71. Sokol S, Moskowitz A, Towle VL. Age-related changes in the latency of the visual evoked potential: influence of check size. Electroencephalogr Clin Neurophysiol. 1981;51(5):559-62.

72. Armstrong RA, Slaven A, Harding GF. Visual evoked magnetic fields to flash and pattern in 100 normal subjects. Vision Res. 1991;31(11):1859-64.

73. Stephen JM, Knoefel JE, Adair J, Hart B, Aine CJ. Aging-related changes in auditory and visual integration measured with MEG. Neuroscience Letters. 2010;484(1):76-80.

74. Price D, Tyler LK, Neto Henriques R, Campbell KL, Williams N, Treder MS, et al. Age-related delay in visual and auditory evoked responses is mediated by white- and grey-matter differences. Nature Communications. 2017;8(1).

75. West KL, Zuppichini MD, Turner MP, Sivakolundu DK, Zhao Y, Abdelkarim D, et al. BOLD hemodynamic response function changes significantly with healthy aging. NeuroImage. 2019;188:198-207.

76. Cliff M, Joyce DW, Lamar M, Dannhauser T, Tracy DK, Shergill SS. Aging effects on functional auditory and visual processing using fMRI with variable sensory loading. Cortex. 2013;49(5):1304-13.

77. Peiffer AM, Hugenschmidt CE, Maldjian JA, Casanova R, Srikanth R, Hayasaka S, et al. Aging and the interaction of sensory cortical function and structure. Hum Brain Mapp. 2009;30(1):228-40.

78. Tekes A, Mohamed MA, Browner NM, Calhoun VD, Yousem DM. Effect of age on visuomotor functional MR imaging. Acad Radiol. 2005;12(6):739-45.

79. Grinband J, Steffener J, Razlighi QR, Stern Y. BOLD neurovascular coupling does not change significantly with normal aging. Hum Brain Mapp. 2017;38(7):3538-51.

80. Aizenstein HJ, Clark KA, Butters MA, Cochran J, Stenger VA, Meltzer CC, et al. The BOLD hemodynamic response in healthy aging. J Cogn Neurosci. 2004;16(5):786-93.

81. Brodtmann A, Puce A, Syngeniotis A, Darby D, Donnan G. The functional magnetic resonance imaging hemodynamic response to faces remains stable until the ninth decade. NeuroImage. 2003;20(1):520-8.

82. Adaikkan C, Middleton SJ, Marco A, Pao P-C, Mathys H, Kim DN-W, et al. Gamma Entrainment Binds Higher-Order Brain Regions and Offers Neuroprotection. Neuron. 2019;102(5):929-43.e8.

83. Iaccarino HF, Singer AC, Martorell AJ, Rudenko A, Gao F, Gillingham TZ, et al. Gamma frequency entrainment attenuates amyloid load and modifies microglia. Nature. 2016;540(7632):230-5.

84. Martorell AJ, Paulson AL, Suk H-J, Abdurrob F, Drummond GT, Guan W, et al. Multi-sensory Gamma Stimulation Ameliorates Alzheimer's-Associated Pathology and Improves Cognition. Cell. 2019;177(2):256-71.e22.

85. Tsoneva T, Garcia-Molina G, Desain P. SSVEP phase synchronies and propagation during repetitive visual stimulation at high frequencies. Scientific Reports. 2021;11(1).

86. Herrmann CS. Human EEG responses to 1-100 Hz flicker: resonance phenomena in visual cortex and their potential correlation to cognitive phenomena. Experimental Brain Research. 2001;137(3-4):346-53.

87. Shibata K, Yamane K, Otuka K, Iwata M. Abnormal visual processing in migraine with aura: a study of steady-state visual evoked potentials. J Neurol Sci. 2008;271(1-2):119-26.

88. Angelini L, de Tommaso M, Guido M, Hu K, Ivanov P, Marinazzo D, et al. Steady-state visual evoked potentials and phase synchronization in migraine patients. Phys Rev Lett. 2004;93(3):038103.

89. Clementz BA, Keil A, Kissler J. Aberrant brain dynamics in schizophrenia: delayed buildup and prolonged decay of the visual steady-state response. Brain Res Cogn Brain Res. 2004;18(2):121-9.

90. Jin Y, Castellanos A, Solis ER, Potkin SG. EEG Resonant Responses in Schizophrenia: a Photic Driving Study with Improved Harmonic Resolution. Schizophrenia Research. 2000;44(3):213-20.

91. Wilson TW, Hernandez OO, Asherin RM, Teale PD, Reite ML, Rojas DC. Cortical gamma generators suggest abnormal auditory circuitry in early-onset psychosis. Cereb Cortex. 2008;18(2):371-8.

92. Wilson TW, Rojas DC, Reite ML, Teale PD, Rogers SJ. Children and adolescents with autism exhibit reduced MEG steady-state gamma responses. Biol Psychiatry. 2007;62(3):192-7.

93. Wilson TW, Wetzel MW, White ML, Knott NL. Gamma-frequency neuronal activity is diminished in adults with attention-deficit/hyperactivity disorder: a pharmaco-MEG study. J Psychopharmacol. 2012;26(6):771-7.

94. Teale P, Collins D, Maharajh K, Rojas DC, Kronberg E, Reite M. Cortical source estimates of gamma band amplitude and phase are different in schizophrenia. Neuroimage. 2008;42(4):1481-9.

95. Albouy P, Martinez-Moreno ZE, Hoyer RS, Zatorre RJ, Baillet S. Supramodality of neural entrainment: Rhythmic visual stimulation causally enhances auditory working memory performance. Sci Adv. 2022;8(8):eabj9782.

96. Pastor MA, Artieda J, Arbizu J, Valencia M, Masdeu JC. Human Cerebral Activation during Steady-State Visual-Evoked Responses. The Journal of Neuroscience. 2003;23(37):11621-7.

97. Taulu S, Simola J. Spatiotemporal signal space separation method for rejecting nearby interference in MEG measurements. Phys Med Biol. 2006;51(7):1759-68.

98. Ille N, Berg P, Scherg M. Artifact correction of the ongoing EEG using spatial filters based on artifact and brain signal topographies. J Clin Neurophysiol. 2002;19(2):113-24.

99. Kovach CK, Gander PE. The demodulated band transform. J Neurosci Methods. 2016;261:135-54.

100. Ernst MD. Permutation Methods: A Basis for Exact Inference. 2004;19(4):676-85.

101. Maris E, Oostenveld R. Nonparametric statistical testing of EEG- and MEG-data. Journal of Neuroscience Methods. 2007;164(1):177-90.

102. Dalal SS, Sekihara K, Nagarajan SS. Modified Beamformers for Coherent Source Region Suppression. IEEE Transactions on Biomedical Engineering. 2006;53(7):1357-63.

103. Gross J, Kujala J, Hamalainen M, Timmermann L, Schnitzler A, Salmelin R. Dynamic imaging of coherent sources: Studying neural interactions in the human brain. Proc Natl Acad Sci U S A. 2001;98(2):694-9.

104. Van Veen BD, van Drongelen W, Yuchtman M, Suzuki A. Localization of brain electrical activity via linearly constrained minimum variance spatial filtering. IEEE Trans Biomed Eng. 1997;44(9):867-80.

105. Hillebrand A, Singh KD, Holliday IE, Furlong PL, Barnes GR. A new approach to neuroimaging with magnetoencephalography. Hum Brain Mapp. 2005;25(2):199-211.

106. Gaser C, Dahnke R, Thompson PM, Kurth F, Luders E. CAT – A Computational Anatomy Toolbox for the Analysis of Structural MRI Data. 2022.

107. Dahnke R, Yotter RA, Gaser C. Cortical thickness and central surface estimation. Neuroimage. 2013;65:336-48.

108. Yotter RA, Dahnke R, Thompson PM, Gaser C. Topological correction of brain surface meshes using spherical harmonics. Human Brain Mapping. 2011;32(7):1109-24.

109. Yotter RA, Thompson PM, Gaser C. Algorithms to improve the reparameterization of spherical mappings of brain surface meshes. J Neuroimaging. 2011;21(2):e134-47.

110. R Core Team. R: A Language and Environment for Statistical Computing. Vienna, Austria: R Foundation for Statistical Computing; 2020.

111. Wickham H. *ggplot2:* Elegant Graphics for Data Analysis. New York: Springer-Verlag; 2016.

112. Hayes AF. Introduction to Mediation, Moderation, and Conditional Process Analysis. 2nd ed. Little TD, editor: The Guilford Press; 2013.

113. Preacher KJ, Hayes AF. SPSS and SAS procedures for estimating indirect effects in simple mediation models. Behav Res Methods Instrum Comput. 2004;36(4):717-31.

114. Mathworks. MATLAB. 2018b ed. Natick, Massachusetts, United States2018.

115. Baron RM, Kenny DA. The Moderator-Mediator Variable Distinction in Social Psychological

Research: Conceptual, Strategic, and Statistical Considerations. Journal of Personality and Social Psychology. 1986;51(6):1173-82.

116. Spooner RK, Wiesman AI, Proskovec AL, Heinrichs-Graham E, Wilson TW. Rhythmic Spontaneous Activity Mediates the Age-Related Decline in Somatosensory Function. Cereb Cortex. 2019;29(2):680-8.

117. Wiesman AI, O'Neill J, Mills MS, Robertson KR, Fox HS, Swindells S, et al. Aberrant occipital dynamics differentiate HIV-infected patients with and without cognitive impairment. Brain. 2018;141(6):1678-90.

118. Lew BJ, McDermott TJ, Wiesman AI, O'Neill J, Mills MS, Robertson KR, et al. Neural dynamics of selective attention deficits in HIV-associated neurocognitive disorder. Neurology. 2018;91(20):e1860-e9.

119. Spooner RK, Wiesman AI, Mills MS, O'Neill J, Robertson KR, Fox HS, et al. Aberrant oscillatory dynamics during somatosensory processing in HIV-infected adults. Neuroimage Clin. 2018;20:85-91.

120. Spooner RK, Wiesman AI, O'Neill J, Schantell MD, Fox HS, Swindells S, et al. Prefrontal gating of sensory input differentiates cognitively impaired and unimpaired aging adults with HIV. Brain Communications. 2020;2(2).

121. Casagrande CC, Lew BJ, Taylor BK, Schantell M, O'Neill J, May PE, et al. Impact of HIV-infection on human somatosensory processing, spontaneous cortical activity, and cortical thickness: A multimodal neuroimaging approach. Human Brain Mapping. 2021;42(9):2851-61.

122. Heinrichs-Graham E, Wilson TW. Is an absolute level of cortical beta suppression required for proper movement? Magnetoencephalographic evidence from healthy aging. Neuroimage. 2016;134:514-21.

123. Heinrichs-Graham E, McDermott TJ, Mills MS, Wiesman AI, Wang YP, Stephen JM, et al. The lifespan trajectory of neural oscillatory activity in the motor system. Dev Cogn Neurosci. 2018;30:159-68.

124. Rossiter HE, Davis EM, Clark EV, Boudrias MH, Ward NS. Beta oscillations reflect changes in motor cortex inhibition in healthy ageing. Neuroimage. 2014;91:360-5.

125. Lachenmayr BJ, Kojetinsky S, Ostermaier N, Angstwurm K, Vivell PM, Schaumberger M. The different effects of aging on normal sensitivity in flicker and light-sense perimetry. Invest Ophthalmol Vis Sci. 1994;35(6):2741-8.

126. Tobimatsu S. Aging and pattern visual evoked potentials. Optom Vis Sci. 1995;72(3):192-7.

127. Onofrj M, Thomas A, Iacono D, D'Andreamatteo G, Paci C. Age-related changes of evoked potentials. Neurophysiologie Clinique/Clinical Neurophysiology. 2001;31(2):83-103.

128. Somervail R, Bufacchi RJ, Salvatori C, Neary-Zajiczek L, Guo Y, Novembre G, et al. Brain Responses to Surprising Stimulus Offsets: Phenomenology and Functional Significance. Cerebral Cortex. 2022;32(10):2231-44.

129. Di Lollo V, Enns JT, Yantis S, Dechief LG. Response latencies to the onset and offset of visual stimuli. Perception & Psychophysics. 2000;62(1):218-25.

130. Kline DW, Baffa G. Differences in the sequential integration of form as a function of age and interstimulus interval. Exp Aging Res. 1976;2(4):333-43.

131. Török B, Meyer M, Wildberger H. The influence of pattern size on amplitude, latency and wave form of retinal and cortical potentials elicited by checkerboard pattern reversal and stimulus onset-offset. Electroencephalogr Clin Neurophysiol. 1992;84(1):13-9.

132. Vassilev A, Manahilov V, Mitov D. Spatial frequency and the pattern onset-offset response. Vision Research. 1983;23(12):1417-22.

133. Wilson JT. Effects of stimulus luminance and duration on responses to onset and offset. Vision Res. 1983;23(12):1699-709.

134. Gaetz W, Roberts TPL, Singh KD, Muthukumaraswamy SD. Functional and structural correlates of the aging brain: Relating visual cortex (V1) gamma band responses to age-related structural change. Human Brain Mapping. 2012;33(9):2035-46.

135. Sannita WG. Stimulus-specific oscillatory responses of the brain: a time/frequency-related coding process. Clin Neurophysiol. 2000;111(4):565-83.

136. Spooner RK, Arif Y, Taylor BK, Wilson TW. Movement-Related Gamma Synchrony Differentially Predicts Behavior in the Presence of Visual Interference Across the Lifespan. Cerebral Cortex. 2021;31(11):5056-66.

137. Wiesman AI, Wilson TW. The impact of age and sex on the oscillatory dynamics of visuospatial processing. NeuroImage. 2019;185:513-20.

138. Wilson TW, McDermott TJ, Mills MS, Coolidge NM, Heinrichs-Graham E. tDCS Modulates Visual Gamma Oscillations and Basal Alpha Activity in Occipital Cortices: Evidence from MEG. Cereb Cortex. 2018;28(5):1597-609.

139. Van Der Werf J, Jensen O, Fries P, Medendorp WP. Gamma-Band Activity in Human Posterior Parietal Cortex Encodes the Motor Goal during Delayed Prosaccades and Antisaccades. The Journal of Neuroscience. 2008;28(34):8397-405.

140. Roux F, Wibral M, Mohr HM, Singer W, Uhlhaas PJ. Gamma-Band Activity in Human Prefrontal Cortex Codes for the Number of Relevant Items Maintained in Working Memory. Journal of Neuroscience. 2012;32(36):12411-20.

141. Wiesman AI, Heinrichs-Graham E, Proskovec AL, McDermott TJ, Wilson TW. Oscillations during observations: Dynamic oscillatory networks serving visuospatial attention. Hum Brain Mapp. 2017;38(10):5128-40.

142. Fries P, Reynolds JH, Rorie AE, Desimone R. Modulation of oscillatory neuronal synchronization by selective visual attention. Science. 2001;291(5508):1560-3.

143. Gray CM, König P, Engel AK, Singer W. Oscillatory responses in cat visual cortex exhibit inter-columnar synchronization which reflects global stimulus properties. Nature. 1989;338(6213):334-7.

144. Gray CM, Singer W. Stimulus-specific neuronal oscillations in orientation columns of cat visual cortex. Proc Natl Acad Sci U S A. 1989;86(5):1698-702.

145. Merker B. Cortical gamma oscillations: the functional key is activation, not cognition. Neurosci Biobehav Rev. 2013;37(3):401-17.

146. Fries P. Neuronal Gamma-Band Synchronization as a Fundamental Process in Cortical Computation. Annual Review of Neuroscience. 2009;32(1):209-24.

147. Başar-Eroglu C, Strüber D, Schürmann M, Stadler M, Başar E. Gamma-band responses in the brain: a short review of psychophysiological correlates and functional significance. International Journal of Psychophysiology. 1996;24(1):101-12.

148. Fries P. Rhythms for Cognition: Communication through Coherence. Neuron. 2015;88(1):220-35.

149. Keil A, Müller MM, Ray WJ, Gruber T, Elbert T. Human gamma band activity and perception of a gestalt. J Neurosci. 1999;19(16):7152-61.

150. Tallon-Baudry C, Bertrand O. Oscillatory gamma activity in humans and its role in object representation. Trends Cogn Sci. 1999;3(4):151-62.

151. Stauch BJ, Peter A, Ehrlich I, Nolte Z, Fries P. Human visual gamma for color stimuli. Elife. 2022;11.

152. Muthukumaraswamy SD, Singh KD. Visual gamma oscillations: the effects of stimulus type, visual field coverage and stimulus motion on MEG and EEG recordings. Neuroimage. 2013;69:223-30.

153. Tan HM, Gross J, Uhlhaas PJ. MEG sensor and source measures of visually induced gamma-band oscillations are highly reliable. Neuroimage. 2016;137:34-44.

154. McCusker MC, Lew BJ, Wilson TW. Three-Year Reliability of MEG Visual and Somatosensory Responses. Cereb Cortex. 2020.

155. Hermes D, Miller KJ, Wandell BA, Winawer J. Stimulus Dependence of Gamma Oscillations in Human Visual Cortex. Cerebral Cortex. 2015;25(9):2951-9.

156. Bartoli E, Bosking W, Chen Y, Li Y, Sheth SA, Beauchamp MS, et al. Functionally Distinct Gamma Range Activity Revealed by Stimulus Tuning in Human Visual Cortex. Current Biology. 2019;29(20):3345-58.e7.

157. Schadow J, Lenz D, Thaerig S, Busch NA, Fründ I, Rieger JW, et al. Stimulus intensity affects early sensory processing: visual contrast modulates evoked gamma-band activity in human EEG. Int J Psychophysiol. 2007;66(1):28-36.

158. Sun L, Castellanos N, Grützner C, Koethe D, Rivolta D, Wibral M, et al. Evidence for dysregulated high-frequency oscillations during sensory processing in medication-naïve, first episode schizophrenia. Schizophr Res. 2013;150(2-3):519-25.

159. Tada M, Nagai T, Kirihara K, Koike S, Suga M, Araki T, et al. Differential Alterations of Auditory Gamma Oscillatory Responses Between Pre-Onset High-Risk Individuals and First-Episode Schizophrenia. Cereb Cortex. 2016;26(3):1027-35.

160. An KM, Ikeda T, Yoshimura Y, Hasegawa C, Saito DN, Kumazaki H, et al. Altered Gamma Oscillations during Motor Control in Children with Autism Spectrum Disorder. J Neurosci. 2018;38(36):7878-86.

161. Chan D, Suk H-J, Jackson BL, Milman NP, Stark D, Klerman EB, et al. Gamma frequency sensory stimulation in mild probable Alzheimer's dementia patients: Results of feasibility and pilot studies. PLOS ONE. 2022;17(12):e0278412.

162. Wiesman AI, Murman DL, May PE, Schantell M, Wolfson SL, Johnson CM, et al. Visuospatial alpha and gamma oscillations scale with the severity of cognitive dysfunction in patients on the Alzheimer's disease spectrum. Alzheimer's Research & Therapy. 2021;13(1).

163. Adaikkan C, Tsai L-H. Gamma Entrainment: Impact on Neurocircuits, Glia, and Therapeutic Opportunities. Trends in Neurosciences. 2020;43(1):24-41.

164. Benussi A, Cantoni V, Cotelli MS, Cotelli M, Brattini C, Datta A, et al. Exposure to gamma tACS in Alzheimer's disease: A randomized, double-blind, sham-controlled, crossover, pilot study. Brain Stimulation. 2021;14(3):531-40.

165. Uusitalo MA, Ilmoniemi RJ. Signal-space projection method for separating MEG or EEG into components. Med Biol Eng Comput. 1997;35(2):135-40.

166. Hoechstetter K, Bornfleth H, Weckesser D, Ille N, Berg P, Scherg M. BESA source coherence: a new method to study cortical oscillatory coupling. Brain Topogr. 2004;16(4):233-8.

167. Papp N, Ktonas P. Critical evaluation of complex demodulation techniques for the quantification of bioelectrical activity. Biomed Sci Instrum. 1977;13:135-45.

168. JASP Team. JASP (Version 0.14.1)[Computer software]. 2020.

169. L. S. Aiken SGW. Interactions Between Continuous Predictors in Multiple Regression. In: McElroy S, editor. Multiple Regression: Testing and Interpreting Interactions: SAGE Publications, Inc.; 1991. p. 9-27.

170. Landau AN, Fries P. Attention samples stimuli rhythmically. Curr Biol. 2012;22(11):1000-4.

171. Heinrichs-Graham E, Wilson TW. Spatiotemporal oscillatory dynamics during the encoding and maintenance phases of a visual working memory task. Cortex. 2015;69:121-30.

172. Neuper C, Pfurtscheller G. Event-related dynamics of cortical rhythms: frequency-specific features and functional correlates. Int J Psychophysiol. 2001;43(1):41-58.

173. Hanslmayr S, Staudigl T, Fellner MC. Oscillatory power decreases and long-term memory: the information via desynchronization hypothesis. Front Hum Neurosci. 2012;6:74.

174. Sannita WG, Bandini F, Beelke M, De Carli F, Carozzo S, Gesino D, et al. Time dynamics of stimulus- and event-related gamma band activity: contrast-VEPs and the visual P300 in man. Clin Neurophysiol. 2001;112(12):2241-9.

175. Koelewijn L, Dumont JR, Muthukumaraswamy SD, Rich AN, Singh KD. Induced and evoked neural correlates of orientation selectivity in human visual cortex. NeuroImage. 2011;54(4):2983-93.

176. Swettenham JB, Muthukumaraswamy SD, Singh KD. Spectral properties of induced and evoked gamma oscillations in human early visual cortex to moving and stationary stimuli. J Neurophysiol. 2009;102(2):1241-53.

177. Springer SD, Wiesman AI, May PE, Schantell M, Johnson HJ, Willett MP, et al. Altered visual entrainment in patients with Alzheimer's disease: magnetoencephalography evidence. Brain Communications. 2022;4(4).

178. Springer SD, Erker TD, Schantell M, Johnson HJ, Willett MP, Okelberry HJ, et al. Disturbances in primary visual processing as a function of healthy aging. Neuroimage. 2023;271:120020.

179. Wiesman AI, Wilson TW. Alpha Frequency Entrainment Reduces the Effect of Visual Distractors. J Cogn Neurosci. 2019;31(9):1392-403.

180. Wiesman AI, Groff BR, Wilson TW. Frontoparietal Networks Mediate the Behavioral Impact of Alpha Inhibition in Visual Cortex. Cereb Cortex. 2019;29(8):3505-13.

181. Heinrichs-Graham E, McDermott TJ, Mills MS, Coolidge NM, Wilson TW. Transcranial direct-current stimulation modulates offline visual oscillatory activity: A magnetoencephalography study. Cortex. 2017;88:19-31.

182. Parker DM, Salzen EA, Lishman JR. Visual-evoked responses elicited by the onset and offset of sinusoidal gratings: latency, waveform, and topographic characteristics. Invest Ophthalmol Vis Sci. 1982;22(5):675-80.

183. Fortune B, Demirel S, Bui BV. Multifocal visual evoked potential responses to pattern-reversal, pattern-onset, pattern-offset, and sparse pulse stimuli. Vis Neurosci. 2009;26(2):227-35.

184. Busch NA, Debener S, Kranczioch C, Engel AK, Herrmann CS. Size matters: effects of stimulus size, duration and eccentricity on the visual gamma-band response. Clinical Neurophysiology. 2004;115(8):1810-20.

185. Edden RAE, Muthukumaraswamy SD, Freeman TCA, Singh KD. Orientation Discrimination Performance Is Predicted by GABA Concentration and Gamma Oscillation Frequency in Human Primary Visual Cortex. The Journal of Neuroscience. 2009;29(50):15721-6.

186. Hoogenboom N, Schoffelen J-M, Oostenveld R, Parkes LM, Fries P. Localizing human visual gamma-band activity in frequency, time and space. NeuroImage. 2006;29(3):764-73.

187. Gaál ZA, Bodnár F, Czigler I. When Elderly Outperform Young Adults—Integration in Vision Revealed by the Visual Mismatch Negativity. Frontiers in Aging Neuroscience. 2017;9.

188. Kline DW, Orme-Rogers C. Examination of stimulus persistence as the basis for superior visual identification performance among older adults. J Gerontol. 1978;33(1):76-81.

189. Kaur V, Walia L, Singh R. Critical Flicker Fusion Frequency: Effect of Age, Gender, Sleep and Display Screens. International Journal of Contemporary Medical Research [IJCMR]. 2020;7.

190. Mewborn C, Renzi LM, Hammond BR, Miller LS. Critical Flicker Fusion Predicts Executive Function in Younger and Older Adults. Archives of Clinical Neuropsychology. 2015;30(7):605-10.

191. Di Lollo V, Arnett JL, Kruk RV. Age-related changes in rate of visual information processing. J Exp Psychol Hum Percept Perform. 1982;8(2):225-37.

192. Kline DW, Nestor S. Persistence of complementary afterimages as a function of adult age and exposure duration. Exp Aging Res. 1977;3(3):191-201.

193. Brunel N, Wang XJ. What determines the frequency of fast network oscillations with irregular neural discharges? I. Synaptic dynamics and excitation-inhibition balance. J Neurophysiol. 2003;90(1):415-30.

194. Buzsáki G, Wang X-J. Mechanisms of Gamma Oscillations. Annual Review of Neuroscience. 2012;35(1):203-25.

195. Miller EK, Lundqvist M, Bastos AM. Working Memory 2.0. Neuron. 2018;100(2):463-75.

196. Funahashi S, Bruce CJ, Goldman-Rakic PS. Mnemonic coding of visual space in the monkey's dorsolateral prefrontal cortex. Journal of Neurophysiology. 1989;61:331-49.

197. Fuster JM, Alexander GE. Neuron activity related to short-term memory. Science. 1971;173:652-4.

198. Salazar RF, Dotson NM, Bressler SL, Gray CM. Content-Specific Fronto-Parietal Synchronization During Visual Working Memory. Science. 2012;338(6110):1097-100.

199. Lundqvist M, Rose J, Herman P, Brincat SL, Buschman TJ, Miller EK. Gamma and Beta Bursts Underlie Working Memory. Neuron. 2016;90(1):152-64.

200. Honkanen R, Rouhinen S, Wang SH, Palva JM, Palva S. Gamma Oscillations Underlie the Maintenance of Feature-Specific Information and the Contents of Visual Working Memory. Cereb Cortex. 2015;25(10):3788-801.

201. Van Ede F, Jensen O, Maris E. Supramodal Theta, Gamma, and Sustained Fields Predict Modality-specific Modulations of Alpha and Beta Oscillations during Visual and Tactile Working Memory. Journal of Cognitive Neuroscience. 2017;29(8):1455-72.

202. Rottschy C, Langner R, Dogan I, Reetz K, Laird AR, Schulz JB, et al. Modelling neural correlates of working memory: A coordinate-based meta-analysis. NeuroImage. 2012;60(1):830-46.

203. Baddeley A. Working memory: looking back and looking forward. Nature Reviews Neuroscience. 2003;4(10):829-39.

204. Riley MR, Constantinidis C. Role of Prefrontal Persistent Activity in Working Memory. Front Syst Neurosci. 2015;9:181.

205. Jensen O, Tesche CD. Frontal theta activity in humans increases with memory load in a working memory task. Eur J Neurosci. 2002;15(8):1395-9.

206. Brookes MJ, Wood JR, Stevenson CM, Zumer JM, White TP, Liddle PF, et al. Changes in brain network activity during working memory tasks: A magnetoencephalography study. NeuroImage. 2011;55(4):1804-15.

207. Proskovec AL, Heinrichs-Graham E, Wilson TW. Load modulates the alpha and beta oscillatory dynamics serving verbal working memory. NeuroImage. 2019;184:256-65.

208. Bastos AM, Loonis R, Kornblith S, Lundqvist M, Miller EK. Laminar recordings in frontal cortex suggest distinct layers for maintenance and control of working memory. Proceedings of the National Academy of Sciences. 2018;115(5):1117-22.

209. Park DC, Lautenschlager G, Hedden T, Davidson NS, Smith AD, Smith PK. Models of visuospatial and verbal memory across the adult life span. Psychology and Aging. 2002;17:299-320.

210. Bopp KL, Verhaeghen P. Aging and verbal memory span: a meta-analysis. J Gerontol B Psychol Sci Soc Sci. 2005;60(5):P223-33.

211. Salthouse TA, Babcock RL, Shaw RJ. Effects of adult age on structural and operational capacities in working memory. Psychol Aging. 1991;6(1):118-27.

212. Mattay VS, Fera F, Tessitore A, Hariri AR, Berman KF, Das S, et al. Neurophysiological correlates of age-related changes in working memory capacity. Neurosci Lett. 2006;392(1-2):32-7.

213. Heinzel S, Lorenz RC, Duong QL, Rapp MA, Deserno L. Prefrontal-parietal effective connectivity during working memory in older adults. Neurobiol Aging. 2017;57:18-27.

214. Billig AR, Feng NC, Behforuzi H, McFeeley BM, Nicastri CM, Daffner KR. Capacity-limited resources are used for managing sensory degradation and cognitive demands: Implications for age-related cognitive decline and dementia. Cortex. 2020;133:277-94.

215. Cappell KA, Gmeindl L, Reuter-Lorenz PA. Age differences in prefontal recruitment during verbal working memory maintenance depend on memory load. Cortex. 2010;46(4):462-73.

216. Reuter-Lorenz PA, Park DC. Human Neuroscience and the Aging Mind: A New Look at Old Problems. The Journals of Gerontology: Series B. 2010;65B(4):405-15.

217. Schneider-Garces NJ, Gordon BA, Brumback-Peltz CR, Shin E, Lee Y, Sutton BP, et al. Span, CRUNCH, and Beyond: Working Memory Capacity and the Aging Brain. Journal of Cognitive Neuroscience. 2010;22(4):655-69.

218. Smith EE, Geva A, Jonides J, Miller A, Reuter-Lorenz P, Koeppe RA. The neural basis of task-switching in working memory: Effects of performance and aging. Proceedings of the National Academy of Sciences. 2001;98(4):2095-100.

219. Rypma B, Prabhakaran V, Desmond JE, Gabrieli JD. Age differences in prefrontal cortical activity in working memory. Psychol Aging. 2001;16(3):371-84.

220. Rypma B, Eldreth DA, Rebbechi D. Age-related differences in activation-performance relations in delayed-response tasks: A multiple component analysis. Cortex: A Journal Devoted to the Study of the Nervous System and Behavior. 2007;43:65-76.

221. Emery L, Heaven TJ, Paxton JL, Braver TS. Age-related changes in neural activity during performance matched working memory manipulation. NeuroImage. 2008;42(4):1577-86.

222. Morcom AM, Henson RNA. Increased Prefrontal Activity with Aging Reflects Nonspecific Neural Responses Rather than Compensation. The Journal of Neuroscience. 2018;38(33):7303-13.

223. Fakhri M, Sikaroodi H, Maleki F, Ali Oghabian M, Ghanaati H. Age-related frontal hyperactivation observed across different working memory tasks: an fMRI study. Behav Neurol. 2012;25(4):351-61.

224. Tran TT, Hoffner NC, Lahue SC, Tseng L, Voytek B. Alpha phase dynamics predict age-related visual working memory decline. NeuroImage. 2016;143:196-203.

225. Lubitz AF, Niedeggen M, Feser M. Aging and working memory performance: Electrophysiological correlates of high and low performing elderly. Neuropsychologia. 2017;106:42-51.

226. Morrison C, Kamal F, Taler V. The influence of working memory performance on event-related potentials in young and older adults. Cognitive Neuroscience. 2019;10(3):117-28.

227. Spooner RK, Taylor BK, Moshfegh CM, Ahmad IM, Dyball KN, Emanuel K, et al. Neuroinflammatory profiles regulated by the redox environment predicted cognitive dysfunction in people living with HIV: A cross-sectional study. EBioMedicine. 2021;70:103487.

228. Spooner RK, Taylor BK, Ahmad IM, Dyball K, Emanuel K, O'Neill J, et al. Mitochondrial redox environments predict sensorimotor brain-behavior dynamics in adults with HIV. Brain Behav Immun. 2023;107:265-75.

229. Wiesman AI, Heinrichs-Graham E, McDermott TJ, Santamaria PM, Gendelman HE, Wilson TW. Quiet connections: Reduced fronto-temporal connectivity in nondemented Parkinson's Disease during working memory encoding. Human Brain Mapping. 2016;37(9):3224-35.

230. Wilson TW, Proskovec AL, Heinrichs-Graham E, O'Neill J, Robertson KR, Fox HS, et al. Aberrant Neuronal Dynamics during Working Memory Operations in the Aging HIV-Infected Brain. Scientific Reports. 2017;7(1):41568.

231. Koshy SM, Wiesman AI, Spooner RK, Embury C, Rezich MT, Heinrichs-Graham E, et al. Multielectrode Transcranial Electrical Stimulation of the Left and Right Prefrontal Cortices Differentially Impacts Verbal Working Memory Neural Circuitry. Cerebral Cortex. 2020;30(4):2389-400.

232. Embury CM, Wiesman AI, Proskovec AL, Heinrichs-Graham E, McDermott TJ, Lord GH, et al. Altered Brain Dynamics in Patients With Type 1 Diabetes During Working Memory Processing. Diabetes. 2018;67(6):1140-8.

233. Nichols TE, Holmes AP. Nonparametric permutation tests for functional neuroimaging: A primer with examples. Human Brain Mapping. 2002;15(1):1-25.

234. Sghirripa S, Graetz L, Merkin A, Rogasch NC, Semmler JG, Goldsworthy MR. Load-dependent modulation of alpha oscillations during working memory encoding and retention in young and older adults. Psychophysiology. 2021;58(2).

235. Baddeley AD, Hitch G. Working Memory. In: Bower GH, editor. Psychology of Learning and Motivation. 8: Academic Press; 1974. p. 47-89.

236. Baddeley A. The episodic buffer: a new component of working memory? Trends in Cognitive Sciences. 2000;4(11):417-23.

237. Vallar G, Di Betta AM, Silveri MC. The phonological short-term store-rehearsal system: patterns of impairment and neural correlates. Neuropsychologia. 1997;35(6):795-812.

238. Friederici AD. The Role of Left Inferior Frontal and Superior Temporal Cortex in Sentence Comprehension: Localizing Syntactic and Semantic Processes. Cerebral Cortex. 2003;13(2):170-7.

239. Awh E, Jonides J, Smith EE, Schumacher EH, Koeppe RA, Katz S. Dissociation of Storage and Rehearsal in Verbal Working Memory: Evidence From Positron Emission Tomography. Psychological Science. 1996;7(1):25-31.

240. Paulesu E, Frith CD, Frackowiak RSJ. The neural correlates of the verbal component of working memory. Nature. 1993;362(6418):342-5.

241. Pavlov YG, Kotchoubey B. Oscillatory brain activity and maintenance of verbal and visual working memory: A systematic review. Psychophysiology. 2022;59(5).

242. Scheeringa R, Fries P, Petersson K-M, Oostenveld R, Grothe I, Norris DG, et al. Neuronal Dynamics Underlying High- and Low-Frequency EEG Oscillations Contribute Independently to the Human BOLD Signal. Neuron. 2011;69(3):572-83.

243. Hermes D, Nguyen M, Winawer J. Neuronal synchrony and the relation between the blood-oxygen-level dependent response and the local field potential. PLOS Biology. 2017;15(7):e2001461.

244. Guran C-NA, Herweg NA, Bunzeck N. Age-Related Decreases in the Retrieval Practice Effect Directly Relate to Changes in Alpha-Beta Oscillations. The Journal of Neuroscience. 2019;39(22):4344-52.

245. Onton J, Delorme A, Makeig S. Frontal midline EEG dynamics during working memory. NeuroImage. 2005;27(2):341-56.

246. Arnau S, Wascher E, Küper K. Age-related differences in reallocating cognitive resources when dealing with interruptions. Neuroimage. 2019;191:292-302.

247. Logothetis NK, Pauls J, Augath M, Trinath T, Oeltermann A. Neurophysiological investigation of the basis of the fMRI signal. Nature. 2001;412(6843):150-7.